Extreme Ultraviolet Light Production from a ZaP Flow Z-Pinch Xenon Plasma

Keith A. Munson

A thesis submitted in partial fulfillment of
the requirements for the degree of

Master of Science in Aeronautics and Astronautics

University of Washington

2007

Program Authorized to Offer Degree: Aeronautics & Astronautics

University of Washington
Graduate School

This is to certify that I have examined this copy of a master's thesis by

Keith A. Munson

and have found that it is complete and satisfactory in all respects,
and that any and all revisions required by the final
examining committee have been made.

Committee Members:

_____

Uri Shumlak

_____

Brian A. Nelson

Date: _____

Signature_____

Date_____

University of Washington

Abstract

Extreme Ultraviolet Light Production
from a ZaP Flow Z-Pinch Xenon Plasma

Keith A. Munson

Chair of the Supervisory Committee:
Associate Professor Uri Shumlak
Department of Aeronautics and Astronautics

The density of features on semiconductor integrated chips (ICs) can increase as the wavelength of the light used for lithography decreases. Present lithography operates at 193 nanometer (nm) wavelength to produce ICs with features at the 65 nm node. By 2014, the semiconductor industry's goal is to operate lithography at the 22 nm node. To accomplish this, an extreme ultraviolet (EUV) light source operating at 13.5 nm wavelength is required, at a power of at least 180 Watts (W). Using xenon gas, the ZaP experiment is expected to produce plasma that will emit EUV radiation at the 13.5 nm wavelength. The ZaP Flow Z-Pinch Experiment is presently studying the effect of sheared flow on gross plasma stability. In the experiment, hydrogen gas has been used to produce plasma with quiescent periods in the magnetic mode activity which are 2000 times longer than other plasma concepts for creating EUV light, with 300 times the volume. Similar results have been found with xenon gas. An EUV detector designed using an AXUV100, silicon/zirconium filtered photodiode with an 11-18 nm band pass is used to detect any EUV emissions within that spectrum and the total power of the emissions. EUV emissions in 17.4% of the Z-pinch have lasted greater than 16 microseconds (μs), with a average power of 550 kilowatts (kW). The total EUV energy deposition potential from 17.4 % of the Z-pinch is 4.50 joules (J), 450 times more energy than is projected to be needed for lithography.

TABLE OF CONTENTS

LIST OF FIGURES

LIST OF TABLES

ACKNOWLEDGMENTS

The author wishes to express sincere appreciation to Uri Shumlak, Brian Nelson, Ray Golingo, Sean Knecht and the ZaP Team for their guidance and assistance in this endeavor, and to his wife Susan and his family and friends for their understanding and support.

Chapter 1

INTRODUCTION

As the desire for ever smaller, more powerful computers continues to rise, the need for semiconductor technology innovation has become very evident. The current semiconductor lithography methods, the process by which integrated circuit designs are imaged onto their silicon wafer, utilize deep ultraviolet light (DUV) at 193 nanometers (nm) to produce features as small as 30 nm through a combination of water immersion and photomasking techniques [1]. The limits of the immersion technique, however, have led the semiconductor industry to seek new lithography techniques.

The expected replacement of DUV immersion lithography is extreme ultraviolet (EUV) light lithography, operating near the 13.5 nm wavelength. EUV lithography is expected to produce features of 15 nm or less, with 10 nm features possible without immersion techniques. The process of EUV lithography is similar to previous optical lithography methods, requiring an EUV source, a mirror to act as a collecting and focusing tool, and photomasks for the chip to be etched [2].

EUV light sources have been particularly challenging to develop. The leading techniques include laser produced plasmas (LPPs) and gas discharge produced plasmas (GDPPs), using either a xenon (Xe) or tin (Sn) plasma. Based on the current development of EUV photomasks, a total EUV power of 180 W at the intermediate focus (IF) of the source collector is required for high volume manufacturing (HVM) of 120 wafers per hour (wph) [3, 4]. This translates to a required power into a solid angle of 2π steradians (sr), or half a sphere, of 400 W for LPPs and 1200 W for GDPPs [5]. Figure 1.1 shows the layout of both sources with collection optics [6]. Additionally, both of these sources must be pulsed

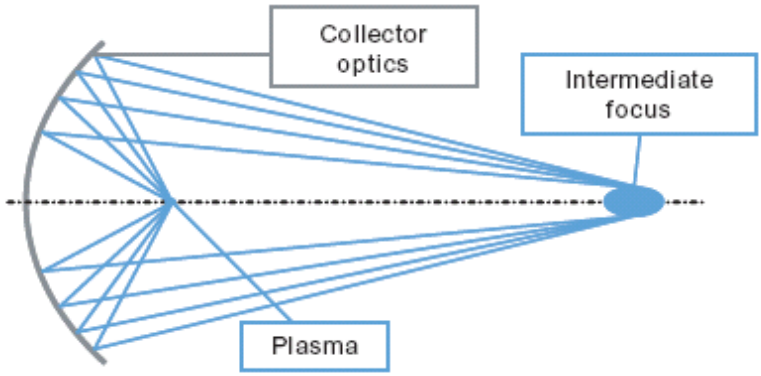

(a)

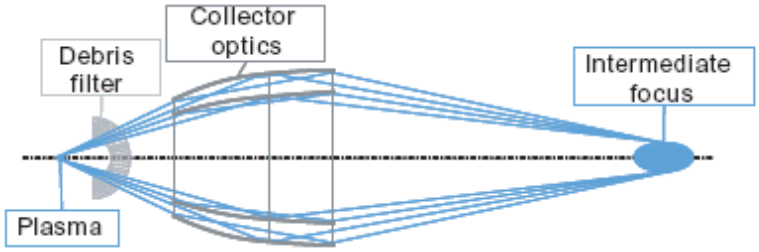

(b)

Figure 1.1: EUV light source collection optics for (a) LPP and (b) GDPP sources. The EUV source radiates into 2π sr, which the collection optics focuses to an intermediate focus, after which the light is applied to photomasks for lithography. A debris filter protects the optics from material liberated by the plasma. The figures are from Stamm (2004), page 3245.

at high repetition rates (1-30 kHz) to develop the required power, due to the short pulse time of between tens and hundreds of nanoseconds [3, 7].

The ZaP Flow Z-Pinch experiment is currently studying the effects of sheared flow on the stability of an otherwise unstable configuration. ZaP has a plasma volume 300 times larger than the approximate volume of 1 cm^3 from both the LPP and GDPP configurations [6, 8]. The duration of the pulse is also 2000 times longer than the pulses found in GDPPs and LPPs [9], making the flow Z-Pinch a potentially good EUV source using a xenon plasma.

The purpose of this thesis is to evaluate the feasibility of using a flow Z-pinch configuration, operating with a xenon plasma, as a EUV light source.

Chapter 2

SUMMARY OF THE ZAP FLOW Z-PINCH EXPERIMENT

2.1 Description of the ZaP Flow Z-Pinch Experiment Setup

The ZaP Flow Z-Pinch experiment is a plasma containment experiment, which takes advantage of a sheared axial plasma flow to stabilize the normally unstable "static" Z-pinch configuration.

ZaP consists of a vacuum tank containing a coaxial plasma accelerator as pictured in Figure 2.1. A 10 cm diameter inner electrode approximately 100 cm long is contained inside a 20 cm diameter outer electrode 200 cm long. Eight gas puff valves are equally spaced around the outer electrode at the midpoint of the inner electrode, $z = -50$ cm, with a single gas puff valve located at the same z location inside the inner electrode. The inner gas puff valve injects gas through a 8 port manifold to give symmetry to the gas injection. Viewports are located at various positions on the experiment, most notably at the point defined as $z = 0$, 17 cm from the end of the nose cone on the inner electrode, where many diagnostic measurements are made. Magnetic probes are inserted axially in the outer electrode 5 cm apart, as well as in azimuthal arrays of 8 probes approximately every 35 cm at $z = 0$, 35 and 70 cm, and in an array of 6 probes at $z = -25$ cm. The purple column in Figure 2.1 represents an idealized Z-pinch plasma column 100 cm long and 2 cm in diameter [8, 9].

2.2 The Physics of the Flow Z-Pinch

The plasma acceleration and containment process is outlined in Figure 2.2. First, a neutral gas such as hydrogen or helium is injected via the 9 gas puff valves. The gas is allowed to a expand for a short period of time, around 1-2 ms, before voltage is applied. Voltage is then applied across the inner and outer electrode by a large external capacitor bank, ranging

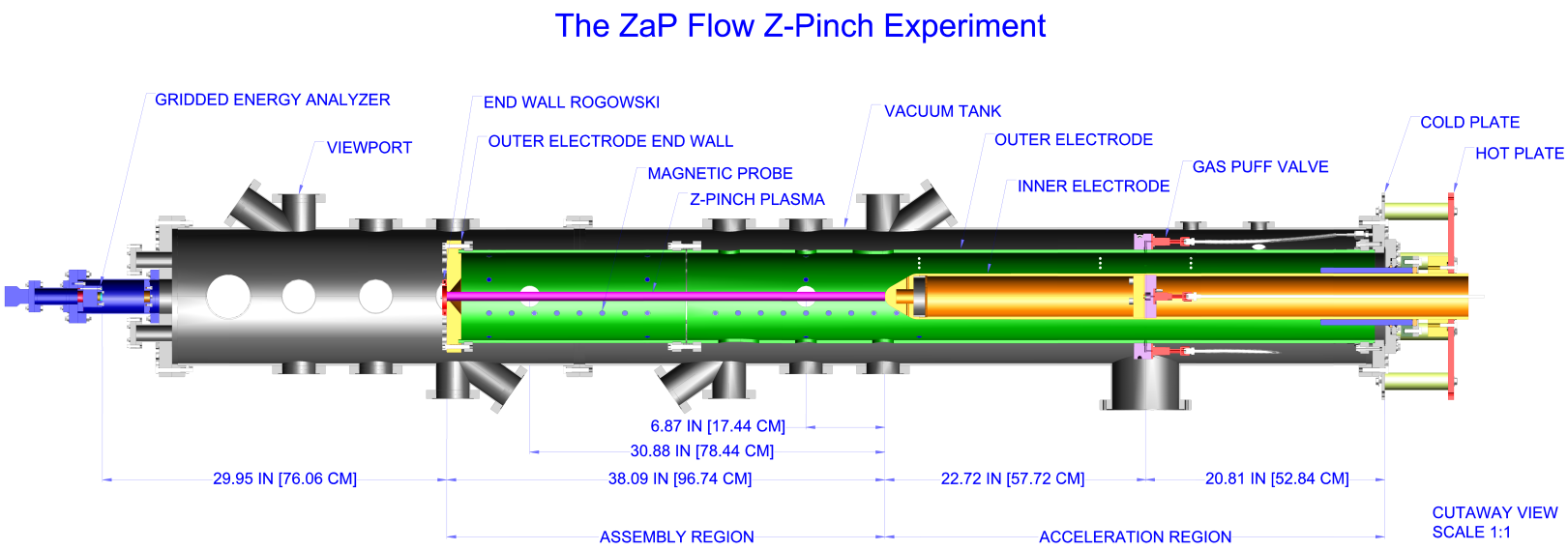

Figure 2.1: Cross Section of the ZaP Flow Z-Pinch Experiment. A vacuum tank contains coaxial electrodes. The inner electrode is 10 cm in diameter and 100 cm long. The outer electrode is 20 cm in diameter and 200 cm long. Nine gas puff valves, one inner and eight outer, inject gas that is ionized and accelerated in the acceleration region to form a Z-pinch in the assembly region. A purple column represents a Z-pinch plasma column that is 1 cm in radius and 100 cm long.

Table 2.1: Typical Flow Z-Pinch operating parameters.

parameter	value
capacitor bank energy	72 kJ (max)
charge voltage	10 kV
total temperature ($T_e + T_i$)	150-200 eV
electron number density (n_e)	10^{17} cm^{-3}
Z-pinch radius	1 cm
Z-pinch length	100 cm
peak current	300 kA

from 1-10 kV, which causes the neutral gas to break down into a plasma. The resulting plasma begins to conduct current, with the current path going from the outer electrode, through the plasma, into the inner electrode, and returning to ground through the end of the inner electrode opposite the nose cone. This results in a J $\times$ B Lorentz force that accelerates the current carrying plasma in the positive z direction along the inner electrode in the region referred to as the acceleration region. As the plasma passes the nose cone, it collapses on axis in the 100 cm long assembly region, where the continued current flow creates an azimuthal magnetic field which continues to pinch the plasma until the pressure of the plasma balances the magnetic pressure, forming a plasma column configuration, giving it the "Z-pinch" name. Neutral gas in the acceleration region continues to ionize and supply the Z-pinch. Typical operating parameters are given in Table 2.1.

2.3 Z-pinch Instabilities

Z-pinches, including the Flow Z-Pinch, have two magnetic instability modes, the $m = 0$ mode or sausage instability, and the $m = 1$ mode or kink instability, which are depicted in Figure 2.3. The sausage instability is caused by a plasma pressure imbalance that allows

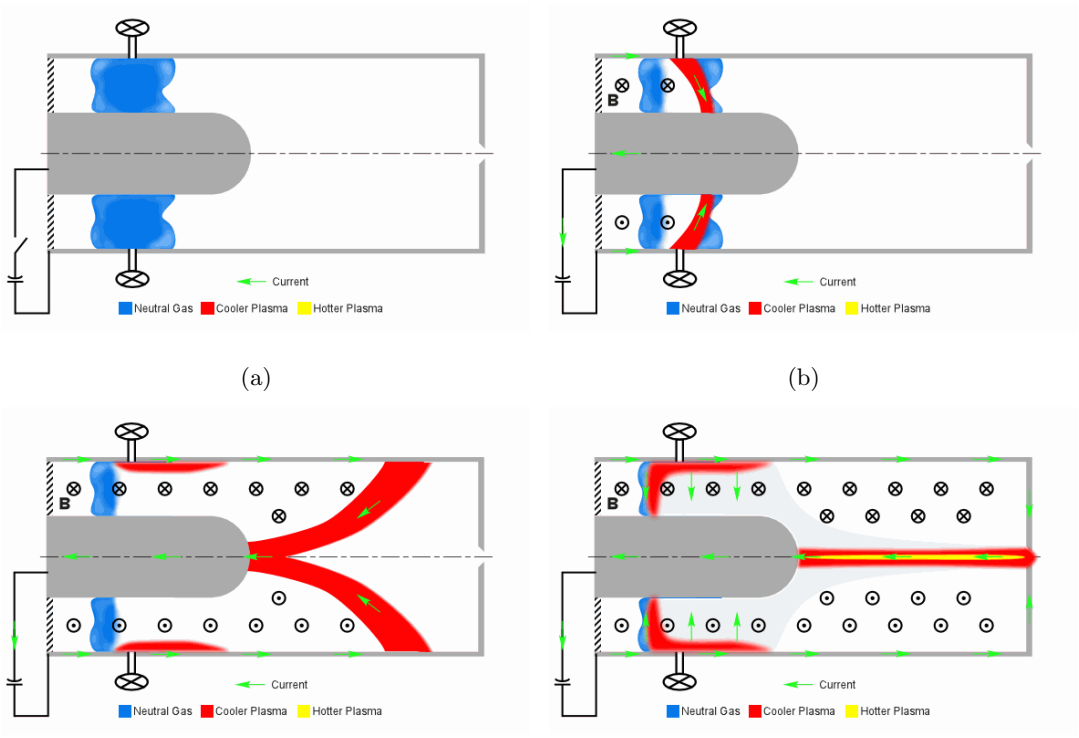

Figure 2.2: Z-pinch formation sequence in a flow Z-pinch. (a) Neutral gas is injected. (b) Voltage is applied across the electrodes, ionizing the gas. Current flows in the plasma from the outer to the inner electrode, then to ground. The resulting magnetic field interacts with the current carrying plasma via the Lorentz force, and accelerates it towards the assembly region. (c) The Z-pinch begins to form as a column of plasma. Current flowing in the Z-pinch generates an azimuthal magnetic field which pinches down on the plasma column until the plasma pressure balances the magnetic pressure. (d) The Z-pinch is formed. Neutral gas still in the acceleration region continues to ionize and supply the pinch.

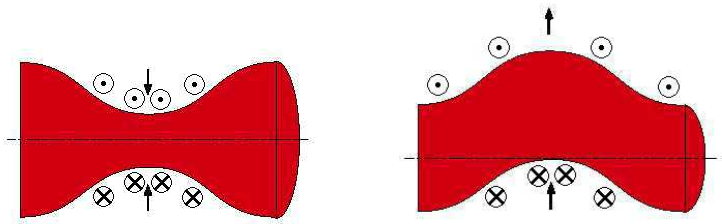

(a) (b)

Figure 2.3: Z-pinch instabilities. (a) $m = 0$ sausage instability. Pressure instabilities in the plasma allow the magnetic field to pinch down on the plasma column, increasing the magnetic field in the region of narrower diameter, increasing the magnetic field until the plasma column current is interrupted. (b) $m = 1$ kink instability. The plasma column begins to kink to one side due to instabilities, and the magnetic field becomes more concentrated on the inside of the kink. This causes the kink to be pushed further away from the main column, until the kink eventually breaks the current flow in the plasma column.

the azimuthal magnetic field to pinch closer to the axis, making the magnetic field stronger, which in turn pinches the plasma column even more until the current flow is interrupted. Kink instabilities similarly form when the plasma column bends to one side, concentrating the magnetic field on the inside of the kink, creating a greater magnetic pressure forcing the kink to become larger until the plasma column is broken.

The radially-sheared axial flow of plasma stabilizes the Z-pinch in the Flow Z-Pinch by comparison to static Z-pinch configurations. This flow has been shown by simulation to stabilize the $m = 0$ mode [10, 11]. The $m = 1$ mode is also stabilized, allowing the Flow Z-Pinch to sustain Z-pinches for 2000 times longer, on the order of 10s of microseconds, as compared to the previously attained lifetime of 10s of nanoseconds in static Z-pinches [8, 9, 11].

The radial shear in the axial flow of the plasma in ZaP occurs during acceleration and formation. Plasma is accelerated to speeds of 100 km/s [9], but the profile of the flow is either faster on the edge or in the middle. Both possibilities stabilize the flow Z-pinch through destructive interference between perturbations in different radial layers of axial flow. This

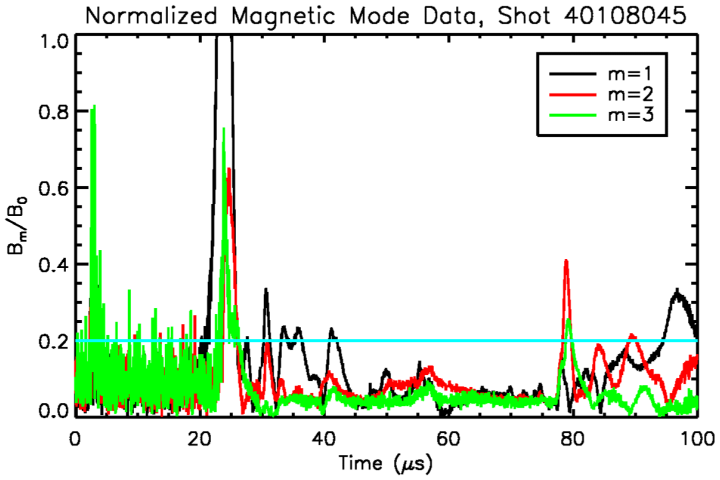

Figure 2.4: Quiescent period as defined by the normalized magnetic mode activity at $z = 0$. The $m = 1$ data remains below 0.2, which corresponds to an approximate 1 cm shift in the current column, from 42 to 79 μs, and the higher modes remain even lower (Shumlak et al., 2006, p. 2).

is true when $\partial V_z/\partial r \geq 0.1kV_A$ where k is the axial wave number, and $V_A = B/\sqrt{\mu_0\rho}$ is the Alfvén speed [8, 9].

2.4 Measurements on the Flow Z-Pinch

Many of the stability measurements of the Flow Z-Pinch come from the magnetic probes mounted in the outer electrode. The magnitude of the time-dependent magnetic field is measured by all magnetic probes, but the Fourier components of the azimuthal arrays can be used to determine the Z-pinch stability. The Fourier components are normalized by the average magnetic field of all the probes. The quiescent period of the Z-pinch, the period during which a stable Z-pinch is sustained, is defined as when the normalized mode $m = 1$ is less than 0.2, and when low order modes ($m = 1, 2, 3$) are low in amplitude and frequency, which also corresponds to a 1 cm shift in the current column [8, 9]. Figure 2.4 depicts the Fourier analyzed normalized mode data. The quiescent period lasts 37 μs for the pulse shown [8].

Other diagnostics for the Flow Z-Pinch include an Imacon fast imaging camera (Imacon) for black and white photographs of the pinch. A charge coupled device (CCD) acts as a time integrated camera attached to a 0.5 m spectrometer which measures specific spectral lines from 200 to 700 nm. Attached to the same spectrometer as the CCD is a photo multiplier tube (PMT) with a small slit that limits the spectral view of the PMT to the full width half maximum (FWHM) of 0.18 nm for time evolution measurements of specific spectral lines. An intensified CCD (ICCD) is connected to another 0.5 m spectrometer for time gated measurements of wavelength bands from 200 to 700 nm. Finally, a solid-state bolometer monitors the emitted power in the band from 0.01 nm to 1100 nm [9, 10, 11].

Chapter 3

XENON PLASMA SURVEY

3.1 Xenon Gas Injection System

To evaluate the Flow Z-Pinch as a viable EUV light source, a xenon gas source has been added to the existing gas injection system. The xenon gas injection system consists of a 100 liter bottle of xenon, a line pressure sensor, a series of valves for isolation and a gas line pump down port, as depicted in Figure 3.1. Each shot activating all 9 gas puff valves of the Flow Z-Pinch experiment uses approximately 10 torr liters of gas, and with a pressure of 801 psig in the bottle, there are 372,400 usable shots with a 100 psig or 5500 torr gas line pressure. The xenon bottle is located directly under the vacuum tank near the end of both electrodes, and contains xenon gas that is 99.999% pure. The distance to the gas injection line has been minimized to minimize the loss of xenon when switching to other gases. The xenon line pressure is monitored via a Baratron pressure transducer. Evacuation of the gas line may be accomplished at the valve board near the vacuum tank, or where the main gas cylinders are connected to the system. Xenon is maintained above atmosphere in the xenon line at all times to prevent impurities from leaking into the line.

3.2 Generation of Xenon Plasma Parameters

With the gas injection system finalized, generation of xenon plasma is possible. Based on operating parameters determined for generating hydrogen plasmas, the operating parameters have been adjusted to create xenon plasmas of similar character as hydrogen plasmas. Parameter surveys have been conducted to determine the optimum parameters based on the magnitude of the magnetic field, and the length of time the normalized mode data remained quiescent.

Line injection pressure was varied first, followed by varying the charge voltage of the

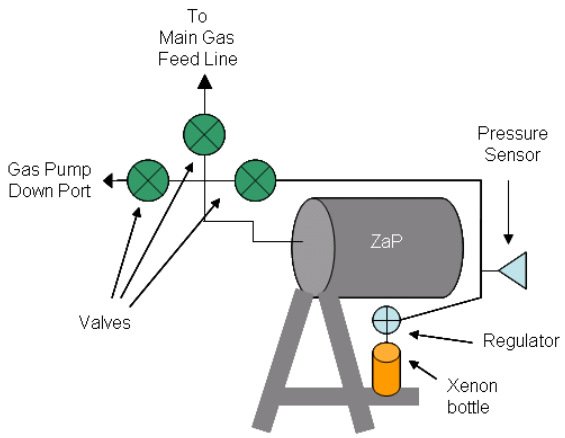

Figure 3.1: The xenon gas injection system has modified the existing gas injection system to allow for xenon gas injection. The xenon gas bottle is mounted below the vacuum tank, with a gas line running to a valve isolation system to allow for switching between xenon and the other injection gases.

capacitor bank used to create plasma and drive current in the Flow Z-Pinch. The configuration of the capacitor bank was then altered to change the inductance of the capacitor bank. Finally, the timing of when the xenon gas was injected was altered.

The pressure survey included xenon line pressures from 2000 to 5500 torr, with a capacitor bank charge voltage of 5 kV. Xenon gas was injected by the inner gas puff valve at $t_{inner} = -1.7$ ms or 1.7 ms prior to applying voltage, and injected by the all the outer gas puff valves at $t_{outer} = -0.8$ ms, which were the optimum settings for hydrogen plasma. One survey was conducted with quarter-gate settings for the gas puff valves. Full-gate valve settings are defined as a 240 dial setting for the inner gas puff valve, and a 60 dial setting for the outer gas puff valves. Quarter settings are a 60 dial setting for the inner gas puff valve, and a 15 dial setting for the outer dial settings. Reducing the dial setting reduces the time during which the gas puff valves are opened, reducing the mass of gas injected. Since a xenon ion is approximately 130 times more massive than a hydrogen ion, a reduction of the mass of plasma to be accelerated was desired until proper settings were determined. The difference in mass results in a factor of 8 reduction in the expansion of the neutral gas

into the vacuum tank, as referenced to the sound speed, and a factor of 11.5 reduction in the Alfvén speed, the characteristic speed in magnetized plasma motion. The results of the initial pressure survey indicated stronger magnetic fields at lower pressure, with a 3000 torr optimum based on the length of the quiescent period.

Next a pressure survey with half gates (inner dial set to 120, outer dials set to 30) was conducted, with the same timing and capacitor bank settings as previously mentioned. At first an optimum of 3750 torr was chosen, but upon further review the 3000 torr setting with quarter gates was a better optimum, and was initially used in the following time surveys.

With the optimum pressure and gate settings determined, the timing of when xenon was injected was altered to increase the magnetic field of the pinch, and to extend the length of the quiescent period. At first, all valve times were altered together, maintaining a 0.9 ms time difference between t_{inner} and t_{outer}, followed by holding $t_{inner} = -1.7$ ms. As the times were moved earlier in time (more negative and further away from the time voltage was applied) the pinch became quiescent for longer periods of time, but with lower magnetic fields, which indicated a more diffuse, colder pinch. Later times (less negative or closer to when voltage was applied) yielded higher magnetic fields, but less quiescent pinches, requiring a time be selected that balanced the output. The optimum setting for t_{outer} was found to be the original -0.8 ms when all the outer valve times were moved together and $t_{inner} = -1.7$ ms. The gate settings were again altered at the optimum timings, and at a fixed bank voltage of 5 kV, and were found to have little effect overall, with a slight increase in the magnitude of the magnetic field at lower gate settings.

After the initial optimization process, the difference between hydrogen and xenon settings was that the amount of xenon gas injected had to be limited by both a lower line pressure (3000 torr vice the 5500 torr for hydrogen) and lower gate settings (quarter vice full). This was due in large part to voltage spikes developed while the Z-pinch was forming and during the quiescent period, which is addressed in the next section.

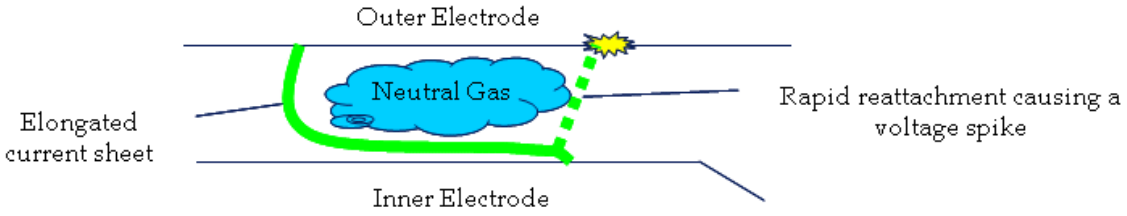

Figure 3.2: An illustration of a xenon plasma blow-by event. The current sheet accelerating the plasma becomes elongated around a neutral pocket of gas, then rapidly reattaches beyond the neutral pocket of gas causing a rapid change in current, and generating a large change in flux resulting in large changes in voltage.

3.3 Observations of Plasma Blow-by Events

Based on the initial survey, xenon plasmas demonstrated more frequent plasma instabilities causing larger changes in the plasma voltage than hydrogen plasmas, which are attributed to the difference in mass between xenon and hydrogen, causing xenon to be more difficult to accelerate smoothly to the assembly region. Aside from the normal sausage and kink instabilities, these plasma instabilities appear to be due in large part to what is referred to as "blow-by" events. A blow-by event occurs when the current sheet accelerating the plasma in the acceleration region becomes elongated around a pocket of neutral gas, then rapidly reattaches on the opposite side of the pocket, creating a surge of flux that causes a short-lived, large plasma voltage spike. A drawing of a blow-by event is given in Figure 3.2.

A blow-by event can also be observed in the magnetic field data, as shown in Figure 3.3. The graph shows a contour plot of the percent of magnetic field at a given z position on the y axis versus time on the x axis, with a plot of the normalized mode data included on the bottom for reference to the quiescence of the pinch. At 20 μs, the majority of the magnetic field is located at $z = -70$ cm. Shortly after the magnetic field contours become almost vertical, indicating the field and the current sheet moved rapidly down the accelerator, reattaching at another z location, before slowing again around 25 μs. Similar events occur

at 60, 65, 73, 80 and 87 μs.

The effect on the Z-pinch by the blow-by event seen in Figure 3.3 is shown in Figure 3.4. The current waveform in the second graph of Figure 3.4 is no longer smooth where a substantial deviation in voltage is seen in the first graph. These large voltage spikes have varying effects on the magnetic field and mode data as well. The largest spike at 73 μs causes a small spike in the magnetic field, but a large change in the magnetic mode data, going from a quiescent to a temporarily unstable Z-pinch. This same effect also occurs at 65 μs. At 80 and 87 μs, there is a substantial increase in the magnetic field following a voltage spike, resulting in a more quiescent pinch.

Overall, blow-by causes instabilities which are unpredictable, and therefore undesirable. Based on the idea of minimizing blow-by, it was decided that the current waveform generated by the capacitor bank was to be altered by increasing the inductance to slow how quickly the current increased in the plasma, and to reduce the plasma voltage spikes observed.

3.4 Changes in the Capacitor Bank Configuration

With the intention of reducing voltage spikes in the xenon plasma, ZaP's main capacitor bank's inductance was increased. Increasing the inductance of the capacitor bank required changing the buss work connecting the capacitors in the capacitor bank. The main capacitor bank consists of eight 170 micro farad (μF) capacitors, and two switching ignitrons. The initial bank configuration is referred to as the pulse forming network (PFN). Four capacitors are connected in parallel with buss bars extending 40.7 cm above the capacitors, then connected to an ignitron. The configuration is mirrored with the other capacitors and ignitron, and the two are connected in parallel to ZaP, giving a total capacitance of 1360 μF. A drawing of one ignitron set of capacitors for the PFN along with the current waveform it generates are given in Figure 3.5.

The inductance of the capacitor bank was initially increased by creating a buss loop 40.7 cm high and 82.6 cm wide, as pictured in Figure 3.6. This medium inductance configuration generated a current waveform with 2 peaks, which were lower in magnitude than the PFN

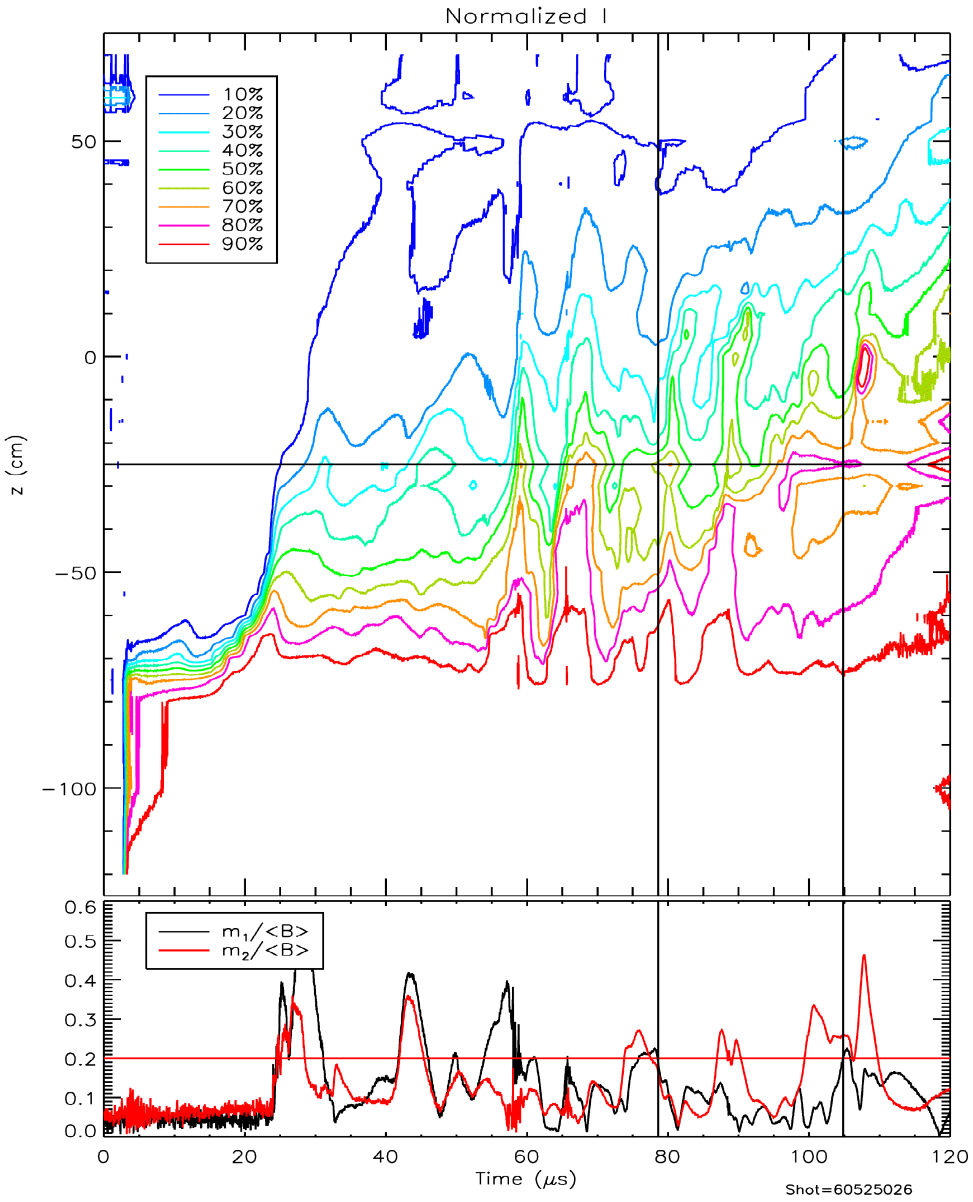

Figure 3.3: Magnetic mode data showing a blow-by event, with the magnetic field at a given z position on the y axis versus time on the x axis, and a plot of the normalized mode data included on the bottom for reference to the quiescence of the pinch. At 20 μs, the majority of the magnetic field is located at $z = -70$ cm. Shortly after the magnetic field contours become almost vertical, indicating the field and the current sheet moved rapidly down the accelerator, showing reattachment at another z location, before slowing again around 25 μs. Similar events occur at 60, 65, 73, 80 and 87 μs.

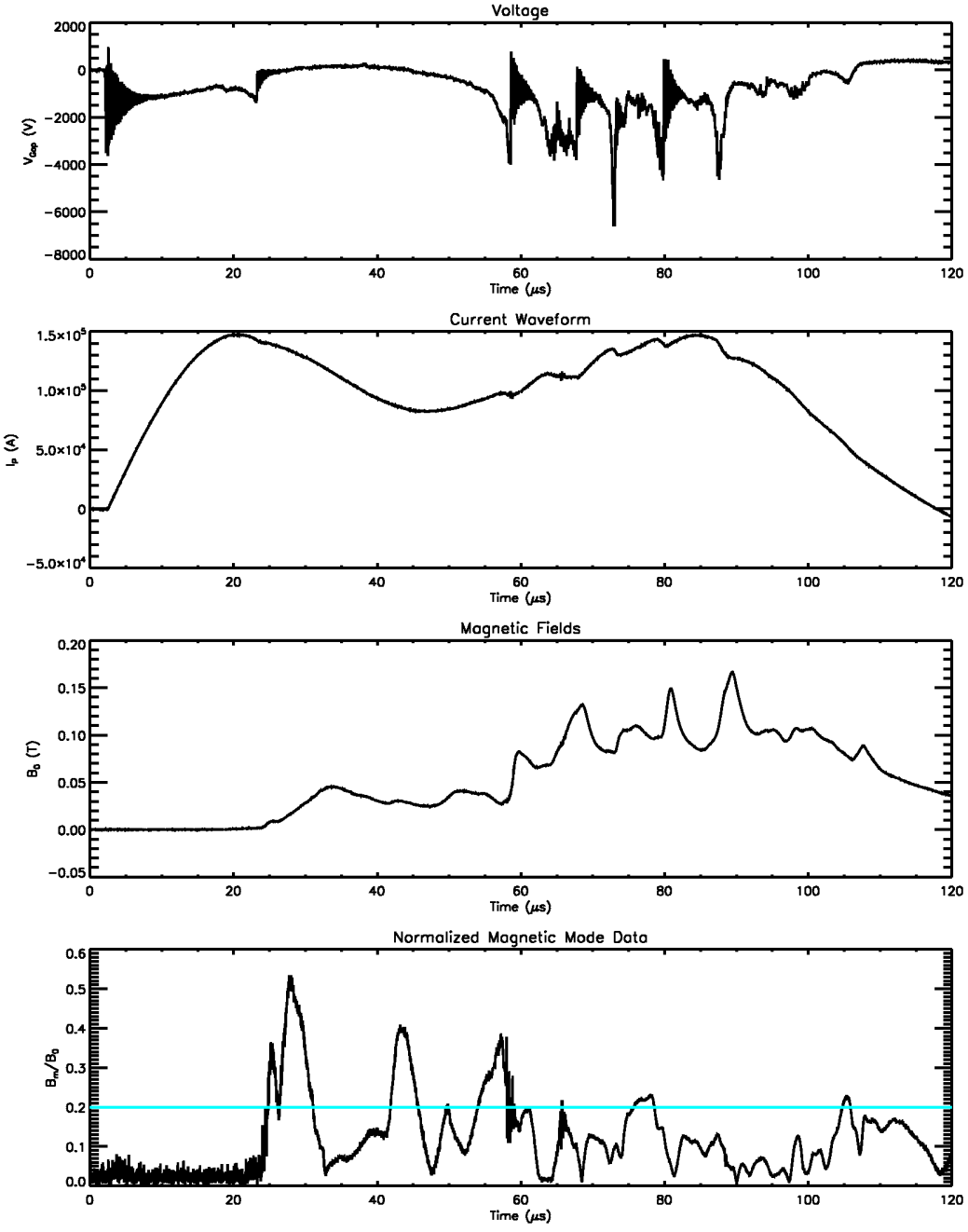

Figure 3.4: Effect of plasma voltage spikes on magnetic field and mode data. Spikes occur at 60, 65, 73, 80 and 87 μs, with a sudden increase in magnetic field, which cause either a sudden increase or decrease in magnetic mode data.

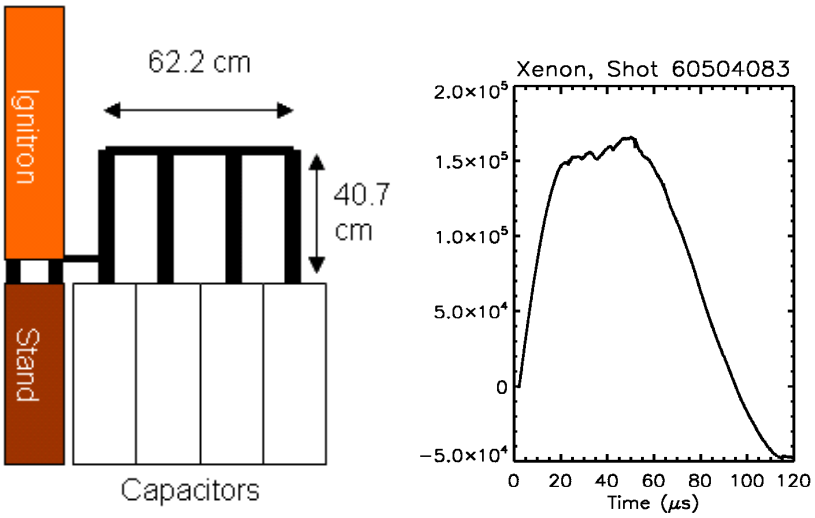

(a) (b)

Figure 3.5: (a) PFN capacitor bank configuration with capacitors connected in parallel via a raised buss of 40.7 cm. (b) The resulting current waveform reaches a peak of 1.65×10^5 A and lasts 95 μs on the positive half cycle.

configuration, and which lasted longer on the positive half cycle, but developed Z-pinches later in time. Magnetic fields in the xenon plasma were stronger, but the quiescent period started later in time, and there were more plasma voltage spikes. Higher capacitor bank voltages were more stable, and an even higher inductance capacitor bank was expected to generate better results.

Increasing the inductance further was accomplished by raising the height of the buss loop to 81.3 cm as drawn in Figure 3.7. The current waveform had 2 peaks again, with a lower minimum between the peaks, and a longer sustained pulse than previously found in the medium inductance configuration. Magnetic fields increased again, but the quiescent period started late, and plasma voltage spikes increased again. Though the increased magnetic field was desirable, the instability of the pinch in this configuration indicated a reduction in capacitor bank inductance was more desirable for a more stable pinch.

Since increasing inductance had not achieved the desired effect, the capacitor bank

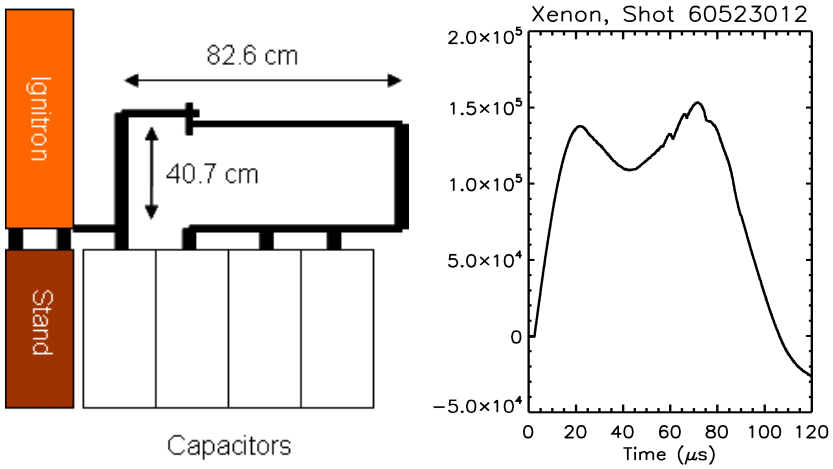

(a) (b)

Figure 3.6: (a) Medium inductance capacitor bank configuration with a buss loop 40.7 cm high and 82.6 cm wide. (b) The resulting current waveform reaches a peak of 1.5×10^5 A, has 2 local maximums, and lasts 105 μs on the positive half cycle.

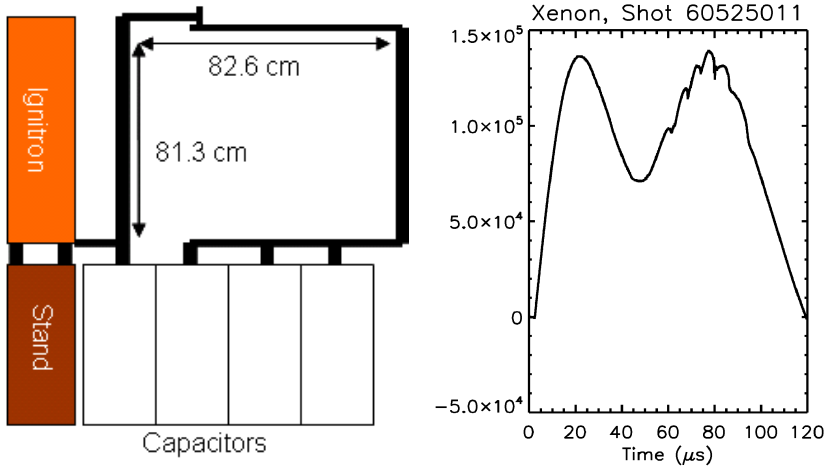

(a) (b)

Figure 3.7: (a) High inductance capacitor bank configuration created with a 82.6 by 81.3 cm buss loop. (b) The resulting current waveform reaches a peak of 1.4×10^5 A, has 2 local maximums, and lasts 120 μs on the positive half cycle, the longest duration of all the configurations.

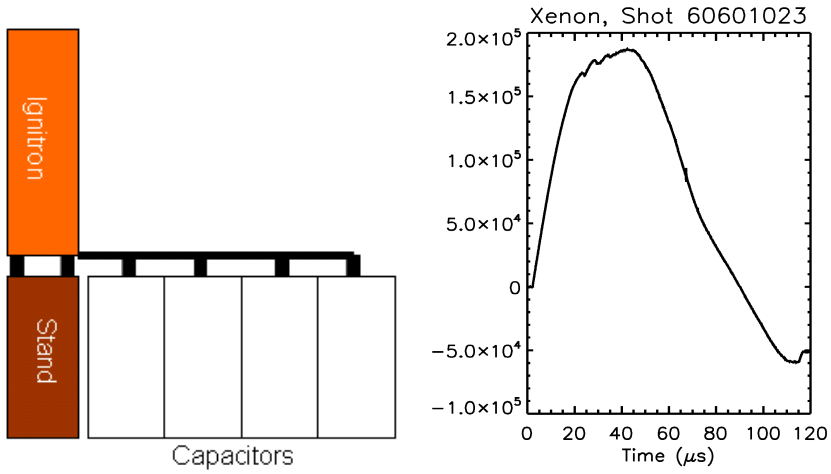

(a) (b)

Figure 3.8: (a) Low inductance capacitor bank configuration with a buss connecting the capacitors with virtually no buss loop. (b) The resulting current waveform reaches a peak of 1.9×10^5 A, the highest peak of all the configurations, and lasts 90 μs on the positive half cycle, the shortest duration of all the configurations.

inductance was lowered from what it had been in the PFN configuration. This was accomplished by eliminating the buss loop and connecting a buss along the top of the capacitors as shown in Figure 3.8. The current waveform reached the highest peak of the attempted configurations, and rose faster than the others as well. It lasted the shortest duration of time, but yielded more quiescent xenon Z-pinches, as well as generating higher magnetic fields. For these reasons, the low inductance bank configuration was chosen as the optimum capacitor bank configuration, and was used for the rest of data taken for xenon plasmas. A comparison of all the bank configurations using identical operating parameters is given in Figure 3.9.

The final portion of the initial xenon plasma survey varied the voltage and gate settings to determine the optimum operating parameters. Lower gate settings with the low inductance configuration were no longer stable, and the gate was optimized at full gates, and 6 kV capacitor bank voltage. The final optimal settings are given in Table 3.1.

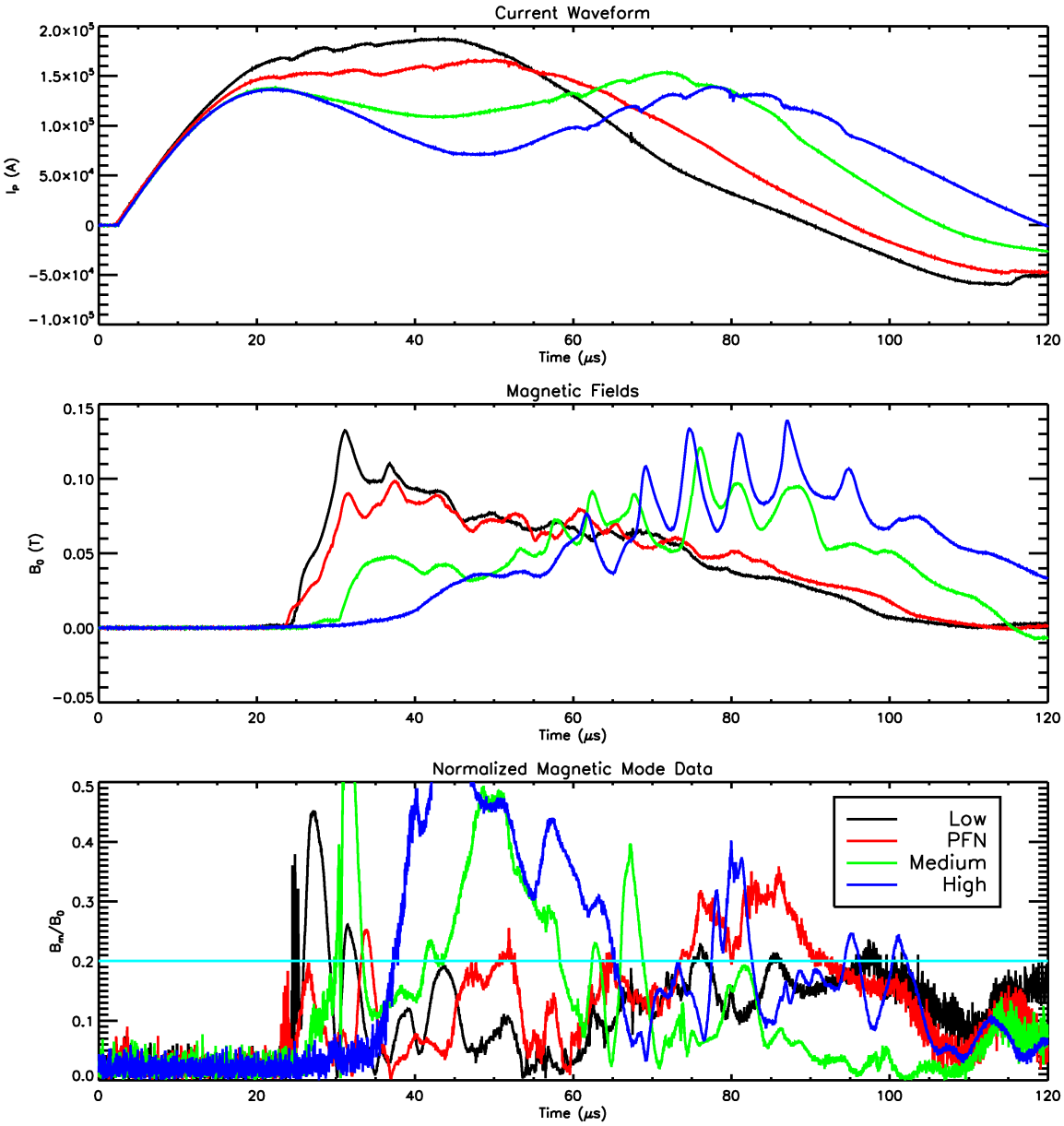

Figure 3.9: Comparison of four different capacitor bank configurations. The legend in the normalized mode data graph on the bottom applies to all 3 graphs. The low inductance bank configuration was chosen as the optimum for its higher current peak, high magnetic fields, and more quiescent pinch.

Table 3.1: Initial Flow Z-Pinch optimum operating parameters for xenon plasmas.

Parameter	Value
Capacitor bank configuration	Low inductance
Charge voltage	6 kV
Line pressure	3000 torr
Gas Puff Valve Gate	Full
t_{inner}	-1.7 ms
t_{outer}	-0.8 ms

3.5 Xenon and Hydrogen Z-Pinch Comparison

With the optimum operating parameters for xenon plasmas determined, the gas was changed in steps back to hydrogen by mixing xenon and hydrogen together. Generally, as the percentage of hydrogen in the gas mix increased, the magnetic fields increased, and the quiescent period became shorter. Finally, ZaP was run with 100% hydrogen with the low inductance bank configuration for comparison to the xenon plasmas created. With similar operating parameters (hydrogen at 6 kV and xenon at 6.5 kV, and all other operating parameters the same) xenon and hydrogen plasmas compare very closely. Figure 3.10 shows Imacon photographs of xenon and hydrogen plasmas taken during their respective quiescent periods. The dark circle on the right of each image is an opening in the outer electrode 4.5 cm in diameter, showing a hydrogen pinch of about 1.5 cm diameter, and a xenon pinch of closer to 2.25 cm diameter [9, 11].

The diameter of the pinches can also be estimated from the ICCD data, also taken during the quiescent period as seen in Figure 3.11. Emissions from the Z-pinch are expected to come from only the main pinch itself, where the plasma is hottest. The ICCD data seen here is taken at 90 degrees to the z axis at $z = 0$, and is aligned radially along the pinch. The width of the ICCD view is marked from 0 (top) to 512 bins (bottom) which corresponds to

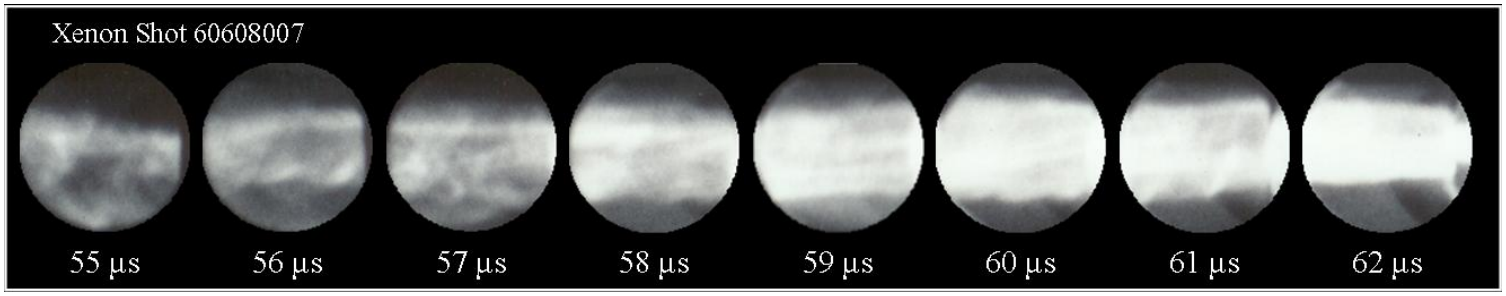

(a)

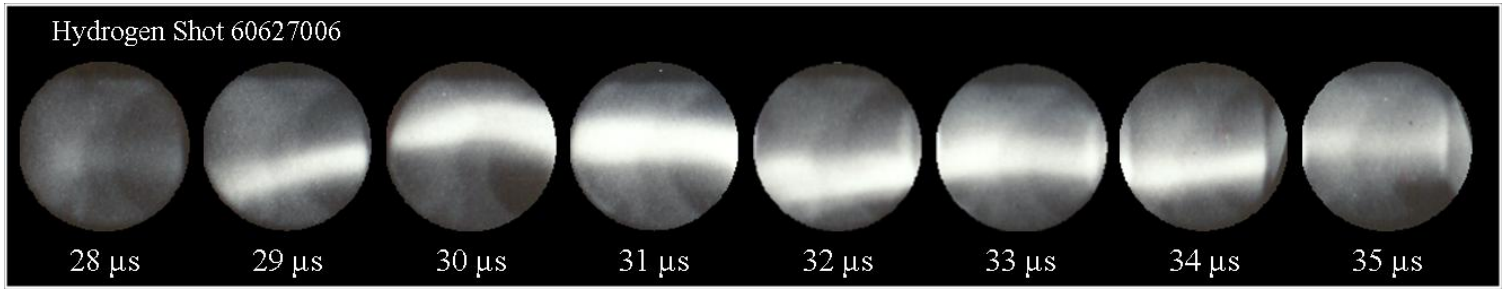

(b)

Figure 3.10: Imacon photographs of hydrogen and xenon Z-pinches taken at $z = 0$ during their respective quiescent periods, with similar operating parameters. The dark circle in the background is an opening in the outer electrode 4.5 cm in diameter. (a) Xenon plasma column using a 6.5 kV charge voltage, with a diameter of 2.25 cm. (b) Hydrogen plasma column using a 6.0 kV charge voltage, with a diameter of 1.5 cm.

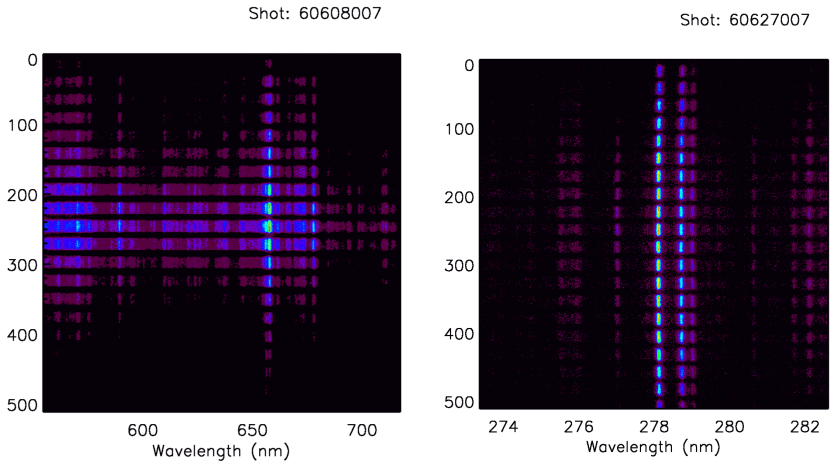

(a) (b)

Figure 3.11: ICCD images of hydrogen and xenon Z-pinches from Figure 3.10. (a) Xenon plasma column using a 6.5 kV charge voltage. The peak occurs at 659 nm, corresponding to a Xe II spectral line, and a pinch radius of 0.65 to 1.5 cm. (b) Hydrogen plasma column using a 6.0 kV charge voltage. The peak occurs at an O V impurity spectral line at 278.1 nm, and indicates a pinch radius of 1 to 1.75 nm. Both pictures also show areas of higher emission going from the blue to the red color spectrum, with red being the highest emission.

a total width of about 3.5 cm [9, 10]. For hydrogen, the ICCD took data at 25 μs for a 10 μs gate, and was centered on a oxygen V line at 278.1 nm, an impurity difficult to remove from any plasma. The long gate covered the entire time pictures were taken in Figure 3.10, and may have also captured movement of the pinch in the lateral or x direction, with the vertical movement shown in Figure 3.10 indicating that lateral movement likely happened, making the pinch appear larger. The xenon ICCD data was taken at 50 μs for a 1 μs gate, centered on 636 nm, and showing a peak at 659 nm which corresponds to a xenon II line. Both correspond to the same shots as shown in Figure 3.10. The hydrogen ICCD data infers a pinch of radius of 1 to 1.75 cm, and the xenon ICCD data infers a pinch radius of 0.65 to 1.5 cm. Both pictures also show areas of higher emission going from the blue to the red color spectrum, with red being the highest emission, which indicates an even smaller diameter of hotter plasma.

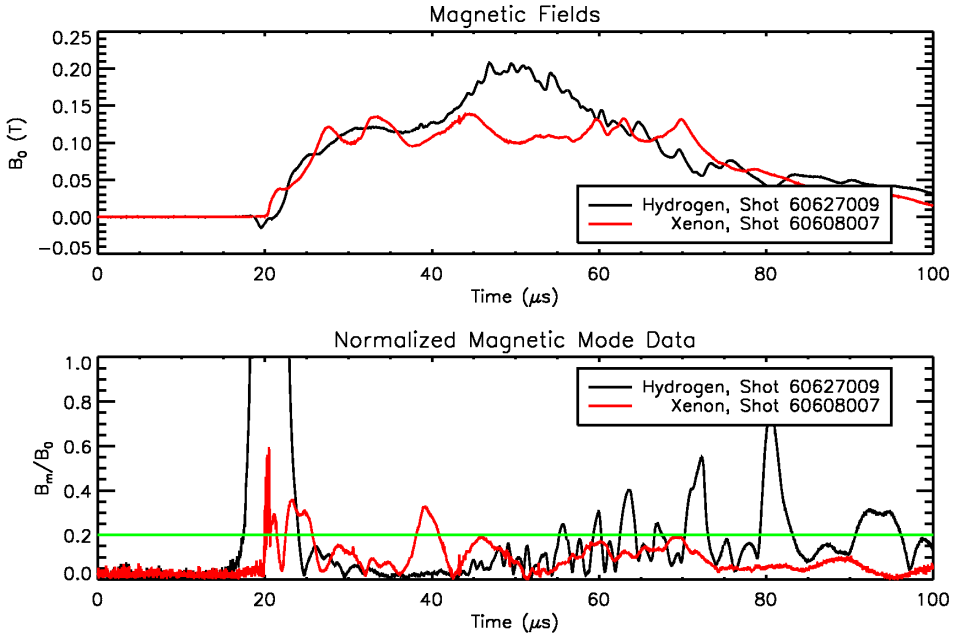

Figure 3.12: Comparison of hydrogen and xenon magnetic field and mode data from the pinches depicted in Figure 3.10. While not always below the 0.2 mode threshold for the quiescent period, the xenon mode data remained lower in frequency and amplitude than the hydrogen after 43 microseconds in time.

The magnetic field data also shows a close comparison of xenon and hydrogen Z-pinches. Figure 3.12 shows the same shots previously depicted by the Imacon photographs in Figures 3.10 and the ICCD images shown in Figure 3.11. The hydrogen Z-pinch has a higher magnetic field, but the duration of the magnetic field is of similar length. Both pinches become quiescent at approximately 25 μs. The frequency and amplitude of the mode data for the hydrogen shot increases after 55 μs, indicating the end of the quiescent period for hydrogen. For the xenon Z-pinch, the mode data remains low in amplitude and frequency except for one short increase in amplitude above the 0.2 limit from 38 to 43 microseconds.

In summary, the xenon Z-pinches generated had quiescent periods which were slightly longer than those for hydrogen plasmas at the same parameters, but with slightly lower magnetic fields. With a mass 130 times larger than the mass of a hydrogen ion, the xenon

plasma was more difficult to accelerate into the assembly region, limiting the capacitor bank voltage due to plasma instabilities such as the blow-by event previously described. A total of 513 xenon data shots were taken during the xenon optimization survey. To measure the EUV output of the xenon Z-Pinch plasma, an EUV diagnostic has been constructed, which is discussed in the next section.

Chapter 4

EUV DIAGNOSTIC DESIGN AND CONSTRUCTION

4.1 Design Considerations for the EUV Diagnostic

With xenon Z-pinches demonstrated in ZaP, a device to measure the EUV production is needed to evaluate ZaP as a possible EUV lithography light source. Previously, the only diagnostic that could measure light in the EUV range was the solid-state bolometer, which can measure all light from 0.04 nm to 1100 nm in wavelength. The bolometer is based around an International Radiation Detector, Inc. (IRD) AXUV100 photodiode, with no filter layer over the sensing portion of the photodiode. The EUV diagnostic is based off the bolometer's design.

To narrow the band of detected light, however, the EUV diagnostic uses a filtered AXUV100 photodiode, with a layer of deposited silicon and zirconium over the 10 mm by 10 mm photosensing area of the diode. This limits the pass band of light to between 11 and 18 nm. Other filtered diodes are available with narrower pass bands, but with lower quantum efficiencies, leading to the selection of the larger pass band to ensure detection of the EUV light, if any.

The design of the EUV diagnostic is based around optimizing the use of the photodiode. The goal is to monitor as much of the Z-pinch as possible while protecting the photodiode from the plasma, and allowing for relatively simple maintenance in the future. Symmetry is used to the maximum extent possible to allow for simple calculations for determining the EUV power measured. Maximum use of the photosensing area is also desired.

ZaP's bolometer is mounted on a 4 5/8" to 2 3/4" reducer conflat, with a 2 3/4" conflat floating-ground BNC feedthrough. A stainless-steel shield surrounds the photodiode, along with a electrostatic shield, with a 40 micron pinhole to limit the amount of light incident on

the diode, and to keep plasma off the diode. The bolometer's photodiode also has a higher quantum efficiency than the filtered diode, so the viewing angle defined by its aperture is smaller compared to the viewing angle of the EUV diagnostic, and attenuation has been used on the bolometer signal. Finally, a simple biasing circuit has been applied to increase the frequency response of the photodiode, a diagram of which is shown later. The biggest drawback of the bolometer's design is the way the shield and diode are mounted to the two conflats prevents removal of the diode or replacement of the pinhole without removing the entire assembly from the vacuum tank.

Based on this one drawback of the bolometer design, the EUV diagnostic is designed such that the 2 3/4" conflat is the mounting base for the photodiode only, while the stainless-steel shield is mounted to the 4 5/8" conflat only, allowing the removal of the photodiode by removing the 2 3/4" conflat. A 50 micron pinhole is used in the EUV diagnostic, and is accessible when the 2 3/4" conflat is removed. Figure 4.1 depicts a cutaway view of the EUV diagnostic.

4.2 Design of the Inner and Outer BNC Holder

Increasing the viewing angle of the photodiode requires placing the photodiode closer to the outer electrode than the bolometer's photodiode. To allow for the replacement of the photodiode in the future, a diode holder consisting of two copper mounts and a teflon socket mount from IRD for the photodiode has been used. The copper mounts are labeled the inner and outer BNC connection in Figure 4.1. The inner BNC holder is for the anode of the photodiode, and connects to the center pin of the floating-ground BNC feedthrough. It measures 1.4 inches long and is 0.8 inches in diameter at its widest point. A total of 6 mounting set screws have been used on the inner holder due to the BNC feedthrough pin not being 90 degrees to the plane of the conflat face, a problem also encountered and corrected for in the bolometer. This ensures the face of the inner holder is parallel to the plane of the conflat. Two holes have been drilled in the face of the inner holder to allow the teflon socket to be mounted on the face of the inner holder. One hole has been oversized to

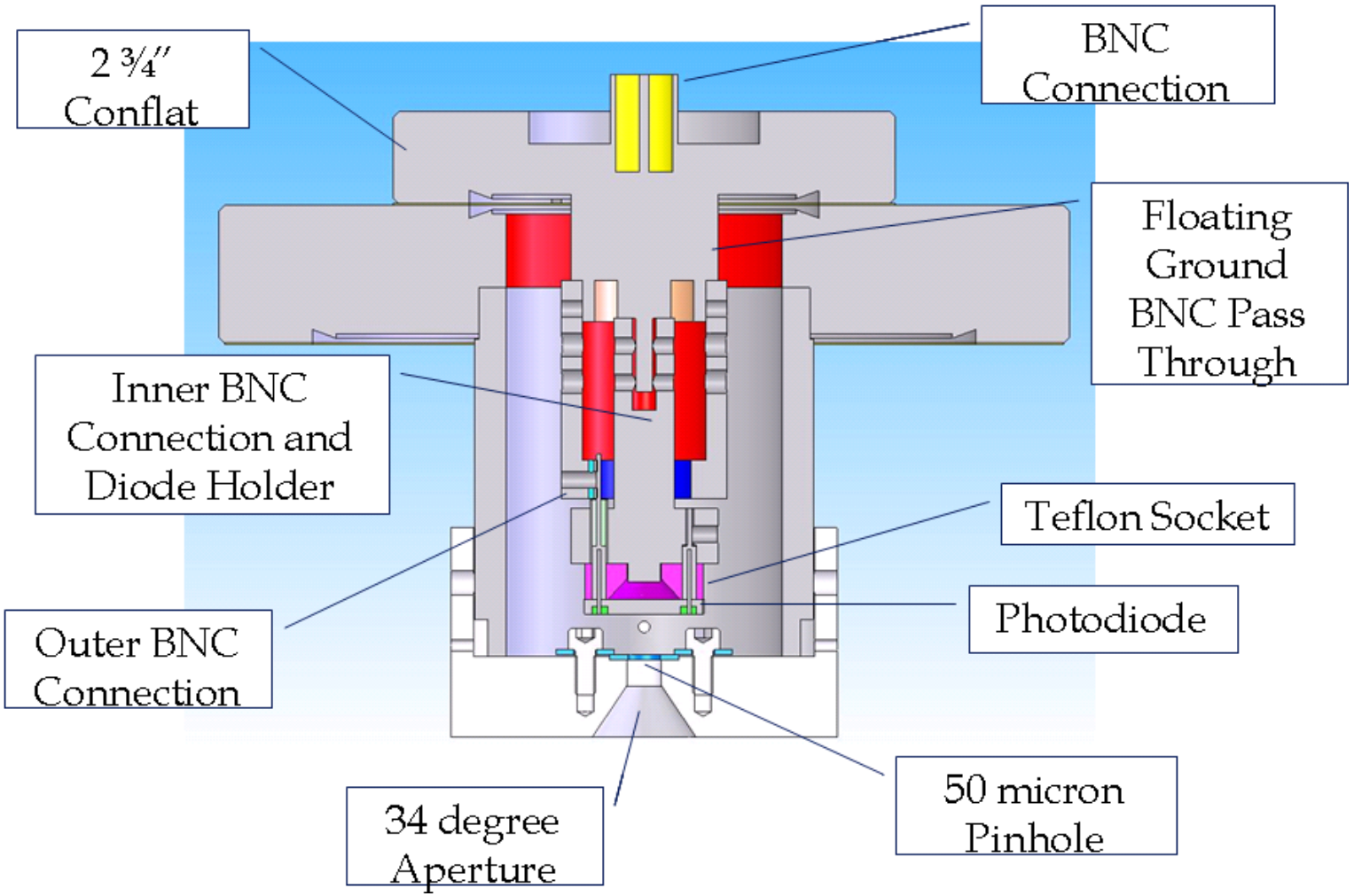

Figure 4.1: Diagram of the EUV diagnostic. The stainless-steel shield is mounted to the 4 5/8" conflat to shield the photodiode from the plasma. The photodiode is mounted to the 2 3/4" conflat to allow removal for replacement of the photodiode, and replacement of the pinhole.

allow the cathode pin of the diode access to the outer holder, and teflon tubing has been used to insulate this pin from the inner holder. The other hole in the face has been drilled out to only slightly larger than the anode pin diameter to allow electrical contact. A set screw has been used to hold the anode pin of the photodiode to the inner holder. A raised copper cylinder on the face of the inner holder is included to center the teflon socket on the face.

The outer BNC holder is a hollow cylinder with one end slightly enclosed, 1.2 inches long, and 0.9 inches in diameter. The inner holder passes through the slightly enclosed end, with a minimum clearance of 50 mils to prevent electrical connection. The cathode pin of the photodiode teflon socket is connected to the slightly enclosed end of the cylinder via a set screw. Six holes have been drilled to allow access to the mounting set screws of the inner holder. Two set screws hold the outer holder to the base of the floating-ground BNC feedthrough on the 2 3/4" conflat. Photographs of both the assembled photodiode holding assembly and its components are shown in Figure 4.2. The entire assembly reaches 2.3 inches above the 2 3/4" conflat face.

4.3 Design of the Photodiode Plasma Shield and Aperture

To protect the photodiode from the plasma and limit the view of the photodiode to a geometrically-symmetric view, a stainless-steel shield has been constructed and mounted to the 4 5/8" conflat. A stainless-steel pipe with an inner diameter of 1.5 inches has been chosen to match the diameter of the hole in the 4 5/8" reducer. This cylinder is cut to 2.0 inch length, and 1.8 inch outer diameter to fit inside a 4 5/8" port on the Flow Z-Pinch, then press fit into the 4 5/8" conflat. The end away from the conflat has a groove cut to a smaller outer diameter to act as a vacuum pump down vent for the shield volume, with 2 small holes drilled into the groove to allow for the pumping out the internal shield volume in the vacuum tank.

A stainless-steel pipe cap has also been machined down to act as the end of the plasma shield, and as the aperture for the photodiode. The inner diameter is slightly oversized to

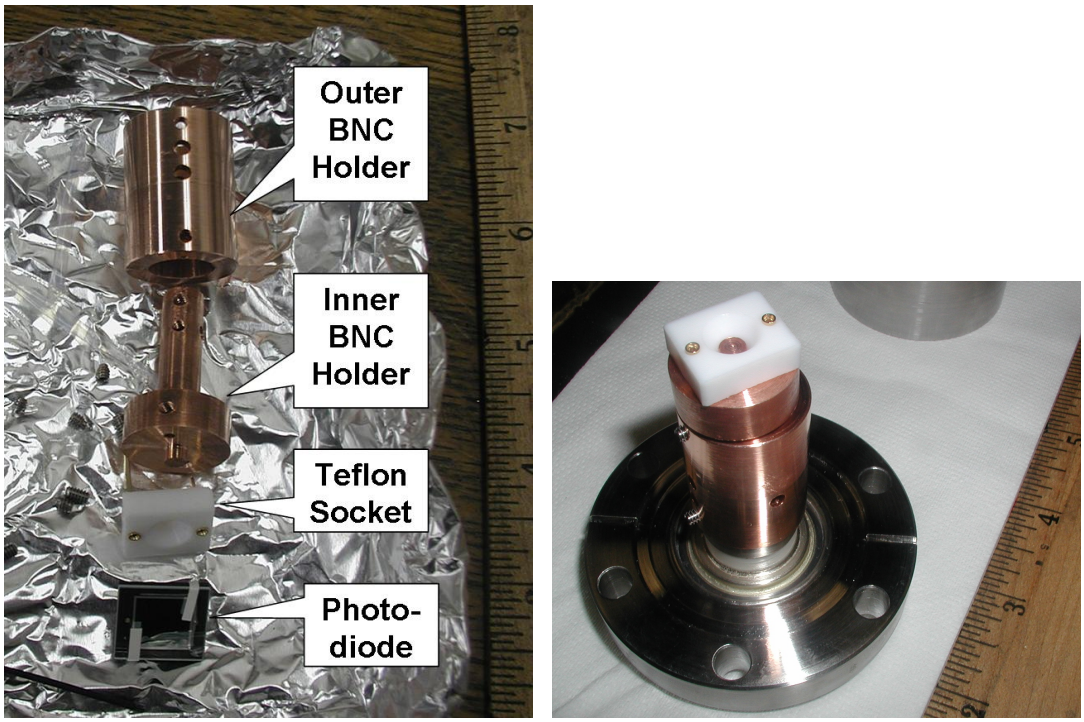

(a) (b)

Figure 4.2: Photographs of the photodiode holding assembly. (a) Exploded view of components. (b) All components except the photodiode mounted on the 2 3/4" floating-ground BNC feedthrough conflat.

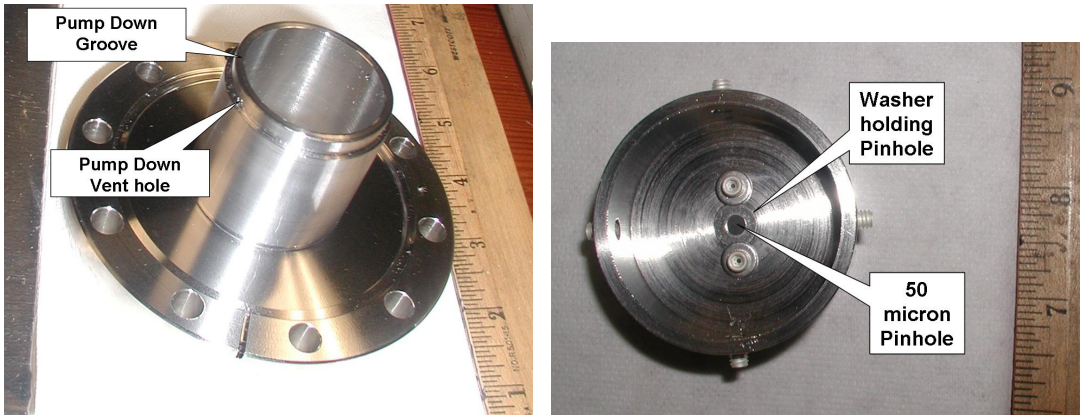

(a) (b)

Figure 4.3: Photographs of the EUV plasma shield. (a) The EUV diagnostic shield with a groove cut in the end for a pump down path through the holes drilled in the groove and in the aperture cap. (b) The aperture holds a 50 micron pinhole, which can be replaced by removing the 2 3/4" conflat while leaving the 4 5/8" conflat in place.

fit the outer diameter of the shield cylinder, and has an outer diameter of 2.1 inches to fit inside a 4 5/8" port on the Flow Z-Pinch. Two holes have been drilled in the side of the cap matching the height of the groove in the cylinder end to allow the pumping out of the internal shield volume. The shield cap is rotated so that the holes in cap are approximately 90 degrees from the holes in the shield cylinder to prevent light leaking through the vacuum pump out path. Four set screws hold the cap to the cylinder, and the face of the shield cylinder rests on the inner face of the cap to ensure the cap face is parallel to the face of the 4 5/8" conflat. A 34 degree aperture is cut in the center of the outside face of the cap, setting the view for the photodiode. A shallow groove has been cut on the inside face of the cap, centering a 50 micron pinhole, with a washer held by two screws holding the pinhole in place. This allows the pinhole to be replaced with out removing the 4 5/8" conflat from the vacuum tank, or the cap from the shield. Some photographs of the shield and aperture assembly are shown in Figure 4.3. The entire shield assembly extends 2.1 inches above the face of the 4 5/8" conflat.

With all components in place, the EUV diagnostic views a cone of 12.86 cm height from the center line of the Flow Z-Pinch, with 17.40 cm diameter base as shown in Figure 4.4. This encompasses 17.4% of the 100 cm long pinch. The EUV diagnostic is currently centered at $z = 17$ cm, 34 cm from the end of the inner electrode, giving it a view of the Z-pinch from $z = 8.3$ cm to $z = 25.7$ cm or from 25.3 to 42.7 cm away from the nose cone of the inner electrode. A biasing circuit applies a -3.6 V bias to the photodiode as pictured in Figure 4.5 to increase the frequency response of the photodiode, and is identical to the biasing circuit used for the bolometer. The AXUV100 Si/Zr photodiodes purchased from IRD have been specifically optimized for the -3.6 V biasing. Great care has been taken to maintain the symmetry and view of the photodiode so that calculations for the power output measured by the EUV diagnostic can be simplified as much as possible. The final step to ensure the proper alignment of the EUV diagnostic is the use of brass shims, five 10 mil shims for the 4 5/8" conflat, and three 7 mil shims for the 2 3/4" conflat. The conflats have been tightened until the shims are all held firmly in place, ensuring the conflats are as parallel as possible to each other, and to the port on the vacuum tank. No floating electrostatic shield is include in this design, but the lack of a floating electrostatic shield has had little impact on the diagnostic's performance, as is discussed in Chapter 5.

4.4 Photodiode Quantum Efficiency Calculation

With the view of the photodiode set, a power calibration factor is needed to relate the current output from the photodiode to the power of EUV light incident on the photodiode, and therefore the EUV power present in ZaP. This is accomplished using the quantum efficiency (QE) of the photodiode. The QE is a ratio of the number of electrons produced by an incident photon in the photosensitive area of the photodiode at a given energy. Figure 4.6 shows the QE of the filtered photodiode used in the EUV diagnostic versus wavelength of light. To calculate the power per unit current detected by the photodiode, multiply the energy of the incident photon by the inverse of the quantum efficiency of that incident photon's wavelength:

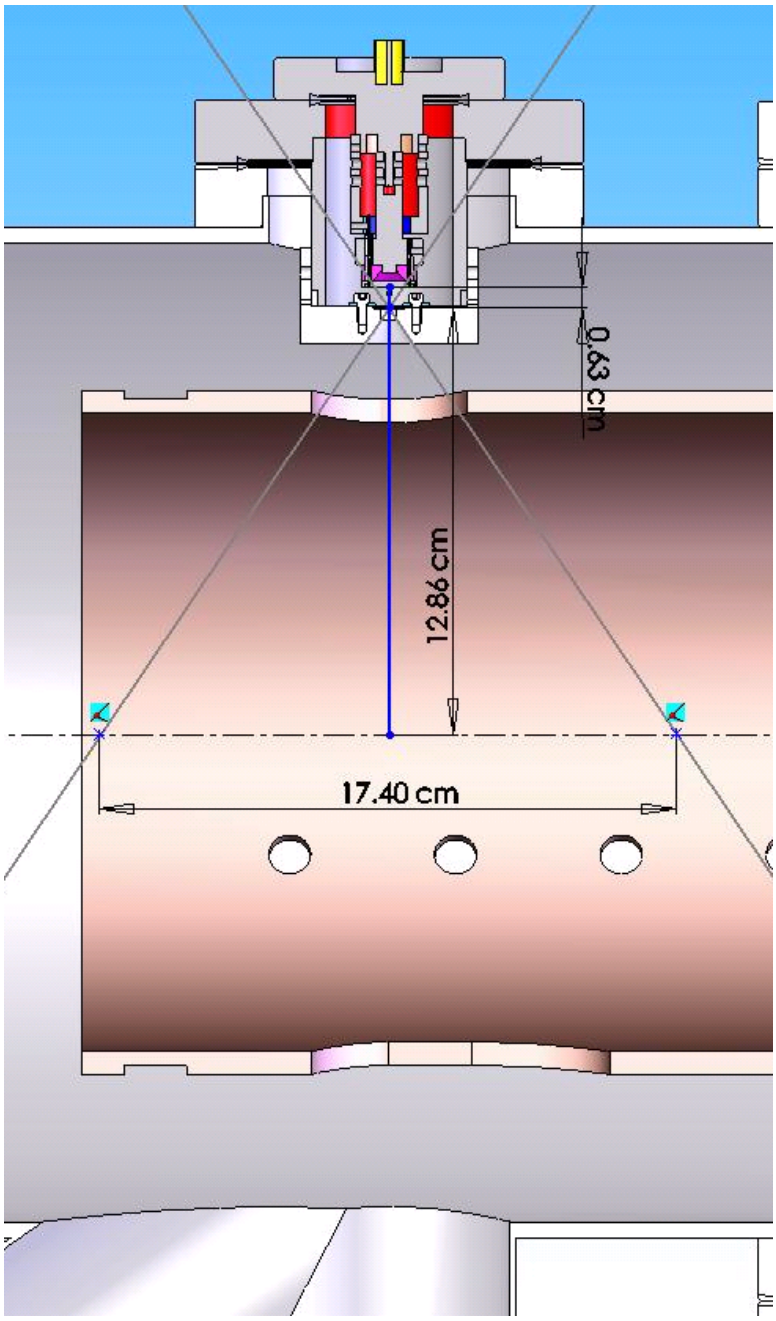

Figure 4.4: Viewing volume of the EUV diagnostic. The diagnostic views a cone 12.86 cm in height from the centerline of the Flow Z-Pinch, with a 17.40 cm diameter base. This allows viewing of 17.4% of the Z-pinch, from $z = 8.3$ cm to $z = 25.7$ cm or from 25.3 to 42.7 cm away from the nose cone of the inner electrode.

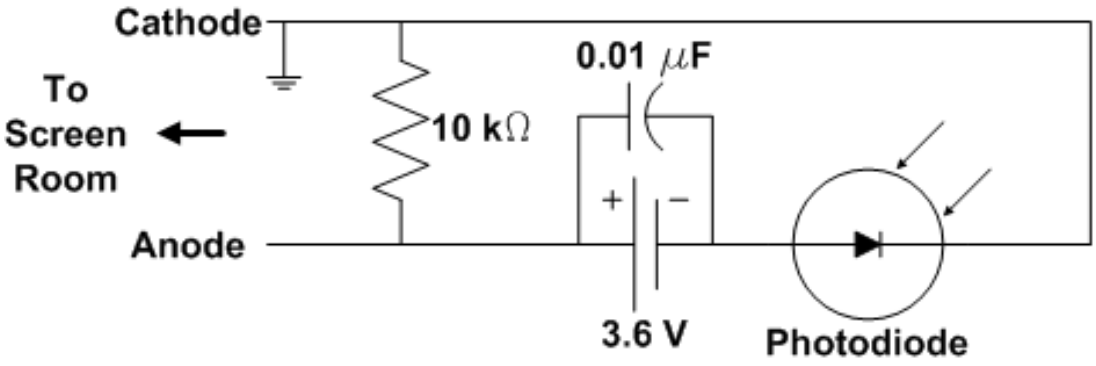

Figure 4.5: Diagram of the photodiode biasing circuit. A −3.6 V battery applies negative biasing to the photodiode to increase its frequency response.

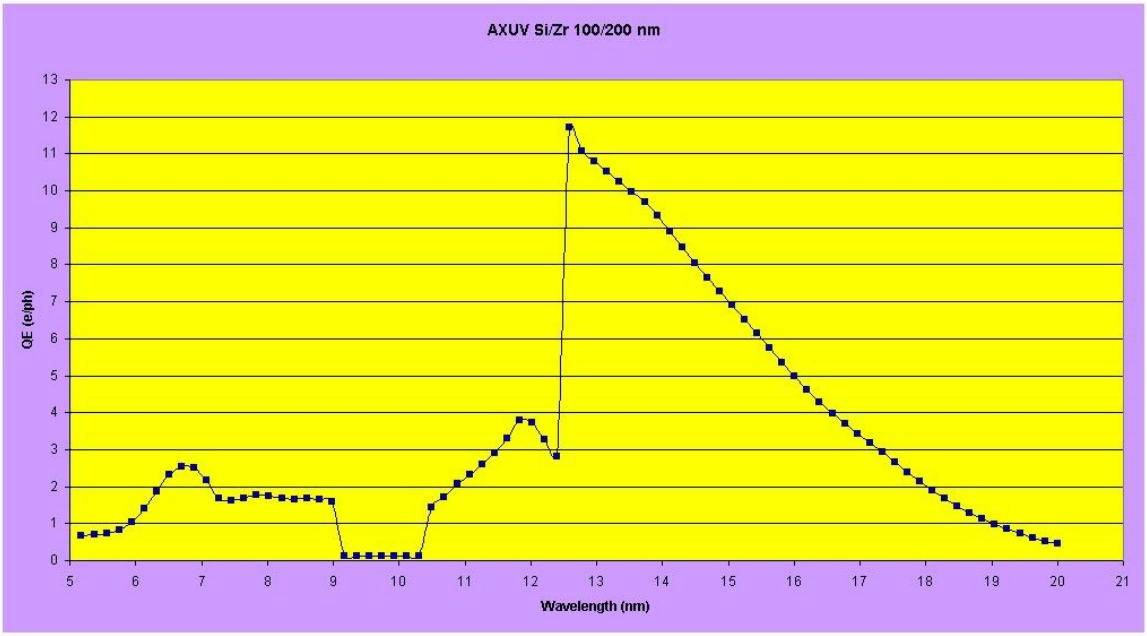

Figure 4.6: Quantum efficiency vs. wavelength of the AXUV100 Si/Zr Photodiode courtesy of IRD. The quantum efficiency relates the current output of the photodiode to the power of EUV light incident on the photodiode.

$$\frac{Energy}{Photon} * \frac{1}{QE} = \frac{Power}{Current} \tag{4.1}$$

From Figure 4.6 the highest QE is 11.79 electrons per photon occurring at 12.59 nm. For a conservative calculation of power output from the Z-pinch, this value has been used as the QE for the photodiode. Finding the energy for the photon at 12.59 nm, the power of EUV light detected per unit current output by the photodiode becomes:

$$\frac{hc}{\lambda} * \frac{1}{QE} = 8.353\ W/A \tag{4.2}$$

Where h is Planck's Constant, c is the speed of light, and λ is the photon's wavelength. This means for every amp of current output from the photodiode, 8.353 watts of incident EUV light power strikes the photosensitive area. This is the lowest power per unit current value from Equation 4.2 in the 11 to 18 nm range based on the IRD QE values, with the average valve in that range being 19.46 W/A. With the EUV power detected per unit current from the photodiode determined, and the viewing volume established for the EUV diagnostic, a power calibration factor for power radiated from the viewed pinch can be determined.

4.5 Solid Angle and EUV Power Calibration Factor Calculation

To calculate the total power emission from the viewed section of the xenon Z-pinch, some simplifications are applied. First, the Z-pinch is assumed to be perfectly cylindrical, with a 1 cm radius. Next, the EUV light is assumed to be emitted from the plasma volume elements only, with no reflections from the tank or inside the detector. From this simplified model, the solid angle from a plasma volume element in the pinch is determined. A solid angle is a two dimensional angle, referenced to the surface area of a sphere of radius 1. Therefore the largest solid angle is 4π steradians or sr. Mathematically, a solid angle is given by:

$$Solid\ Angle = \Omega = \int\int_{Surface} \frac{\hat{n} \cdot d\vec{a}}{r^2} \tag{4.3}$$

Where $\hat{n}$ is the unit normal vector to area $d\vec{a}$, and r is the distance between the origin of the solid angle and the area $d\vec{a}$. Converting the components of Equation 4.3 into Cartesian

coordinates:

$$\hat{n} \cdot d\vec{a} = \cos\theta dxdy \tag{4.4}$$

$$r^2 = x^2 + y^2 + z^2 \tag{4.5}$$

$$\cos\theta = \frac{y}{r} = \frac{y}{\sqrt{x^2 + y^2 + z^2}} \tag{4.6}$$

And substituting Equations 4.4 through 4.6 into Equation 4.3, then evaluating the integral:

$$\Omega = \frac{y * A}{(x^2 + y^2 + z^2)^{\frac{3}{2}}} \tag{4.7}$$

Where A represents the area subtended by the solid angle, which in this calculation is the area of the pinhole where the emission is detected, if it is assumed the area of the pinhole is small and far away from the source of the emission, so as to represent only a small portion of the surface of a sphere that would therefore be approximately flat. Graphically, this solid angle is represented in Figure 4.7.

The power detected can then be related to the power radiated as follows:

$$P_{detected} = \frac{\Omega}{4\pi} P_{radiated} \tag{4.8}$$

Where $\frac{\Omega}{4\pi}$ represents the fraction of the total power radiated actually detected. To determine the total power radiated, Equation 4.8 was solved for $P_{radiated}$, taking into account all the emissions from the entire plasma volume as in Figure 4.7. The $P_{radiated}$ then becomes:

$$P_{radiated} = \frac{4\pi}{The\ solid\ angles\ of\ all\ plasma\ volume\ elements} * Volume * P_{detected}$$

$$P_{radiated} = \frac{4\pi}{\int\int\int_{volume} \Omega dV} * \pi r^2 l * P_{detected} \tag{4.9}$$

Using the Flow Z-Pinch coordinate system as noted in Figure 4.7, with the origin located on the centerline of the pinch directly below the pinhole of the EUV detector, and the z axis aligned along the centerline of the cylinder volume, the solid angle becomes:

$$\Omega = \frac{A(L - y)}{((L - y)^2 + x^2 + z^2)^{\frac{3}{2}}} \tag{4.10}$$

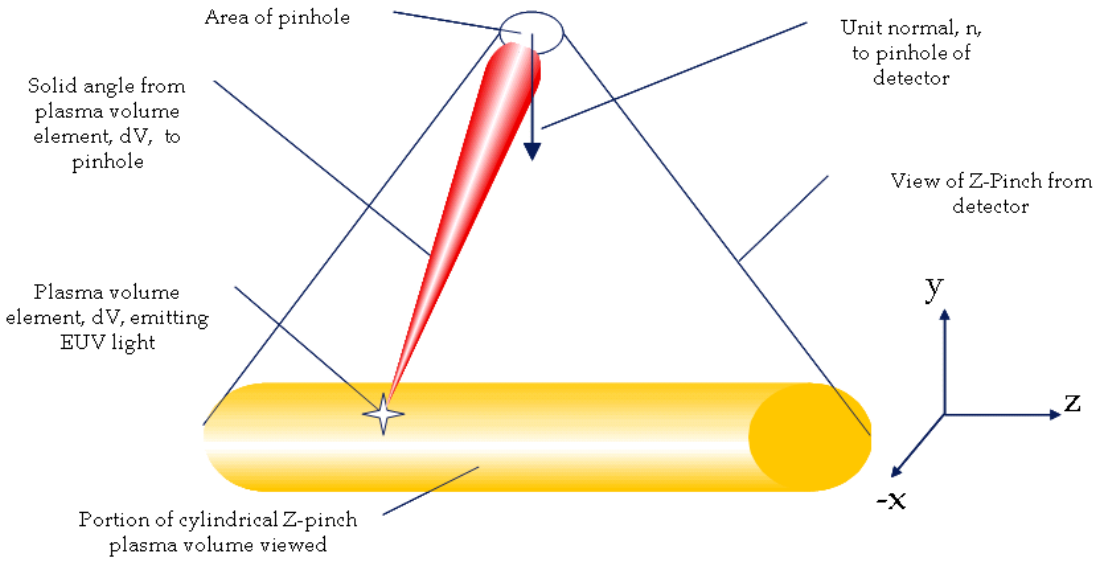

Figure 4.7: Graphical representation of a solid angle. An element of the plasma volume, dV, emits into a solid angle defined by the area of the pinhole, and the distance to the pinhole from the volume element. Cartesian coordinates are used with the origin being on the centerline of the cylinder volume directly below the pinhole, and the z axis aligned on the centerline.

Where L is the radius of the detector, 12.86 cm, and A is the surface area of the pinhole face, 1.96×10^{-5} cm^2. The volume of the viewed pinch has $r = 1$ cm and $l = 17.4$ cm for a total volume in the Z-pinch viewed of 54.7 cm^3. Substituting Equation 4.10 into Equation 4.9, and using the following limits of integration:

$$-\sqrt{1\ cm^2 - y^2} \leq x \leq \sqrt{1\ cm^2 - y^2}$$

$$-1\ cm \leq y \leq 1\ cm$$

$$-(8.7\ cm - 0.675y) \leq z \leq (8.7\ cm - 0.675y)$$

Then multiplying by the power per current factor found in Equation 4.2, the power calibration factor can be found. The limits for the z variable assume that the pinhole allows a view of the plasma column that is straight on either end, which is not completely true. The impact of this assumption, however, is very small, as it changes the total volume viewed by less than a percent, and the though the volume is reduced, the solid angle integral would also be smaller offsetting the change in volume. Finally, the solid angle integral has been evaluated numerically due to the complexity of the expression, giving a power calibration factor (PCF) to 2 significant figures of:

$$PCF = 1.1 \times 10^9\ W/A \tag{4.11}$$

Meaning for every amp of current from the EUV diagnostic, there is 1.1×10^9 W of emitted EUV light power between wavelengths 11–18 nm, from the section of the Z-pinch viewed by the EUV diagnostic, from $z = 8.3$ nm to $z = 25.7$ nm, or from 25.3 to 42.7 cm away from the nose cone of the inner electrode. With the PCF determined, the EUV diagnostic has been used to measure EUV light emission from xenon Z-Pinches, which is discussed next.

Chapter 5

EUV EMISSION SURVEY

5.1 Overview of EUV Light Emission Survey

The EUV diagnostic was installed on the top of the ZaP vacuum tank at position $z = 17$ cm, 34 cm from the tip of the nose cone of the inner electrode. The bolometer which had been installed at that position was moved to the same z position but opposite the EUV diagnostic on the bottom of the vacuum tank. The capacitor bank remained in the low inductance bank configuration through out the EUV emission survey, and pressure, voltage, and gas injection timing were varied to determine the optimal parameters for maximum EUV emission.

First, the timings were set to the optimum found in the initial xenon survey, as noted in Table 3.1. Line pressure was set to 3000 torr, and the gas puff dials were all set to the half-gate setting. The voltage was varied, demonstrating an increase in EUV production with an increase in voltage, with an optimum at 5 kV charge voltage. Next, the gas puff dial settings were increased to the full-gate setting, and the voltage was varied again. Again EUV production increased with voltage, but was optimum at 7.5 kV, with limited data points.

For the next survey, the line pressure was increased to 5500 torr, with all other settings held constant. The voltage was varied starting at 7.5 kV, and increased to 9 kV, but the pinch became too unstable, and the current output due to the voltage spikes prevented constant operation at the higher charge bank voltage. Capacitor bank voltage was then lowered to 7 kV and held constant while the inner gas puff timing was altered. This setting generally led to lower magnetic fields and a less quiescent pinch, and very low EUV production.

The line pressure was again reduced to 3000 torr to increase the EUV production, and the gas puff dial setting was reduced to the half-gate setting to reduce the amount of xenon injected in an effort to develop hotter Z-pinches, with higher magnetic fields and EUV production than had been seen at the high line pressure of 5500 torr. The voltage was varied again, with the highest EUV production and the most quiescent pinches coming at 6 kV charge voltage. The gas puff dial setting was again reduced to the quarter setting, but EUV production and magnetic field strength decreased, so the dial setting was set to the half-gate setting again.

While using the optimum of 6 kV charge voltage with the half gates and holding the inner gas puff timing at -1.7 ms, the outer gas puff timings were all varied together. EUV production increased as the timing was moved later in time (closer to when voltage was applied, or less negative), but the plasma voltage spikes became more pronounced. To mitigate the plasma voltage spikes but allow for later outer gas puff timings, the gas puff dial settings were again increased to the full setting. The plasma voltage spikes were partially stabilized with the full-gate settings, but EUV production went down at later times.

The outer times were then set to the original optimum of -0.8 ms, and the inner gas puff timing was altered. Again, EUV production and magnetic fields increased as the timing was set later, as did the plasma voltage spikes. An optimum of -1.6 ms was chosen for the inner gas timing. Next, a new outer gas puff timing configuration was attempted. Instead of moving all outer gas puff timings together, half were held constant at -0.7 ms and half were varied together. The series of eight outer gas puff valves are controlled in pairs which are opposite to each other around the outer electrode. These controllers are referred to as "gas puff boxes" or GPB's, and the outer gas puff valves correspond to GPB2-5 with GPB1 being the inner gas puff valve control box. For this survey, GPB2 and GPB4 were varied while GPB3 and 5 were held at -0.7 ms. As GPB2 and 4's timings were moved earlier in time, the EUV production and magnetic field increased, with a maximum production occurring at GPB2 and 4 set to -5.0 ms. This gas injection timing configuration created a background fill pressure, as illustrated in Figure 5.1.

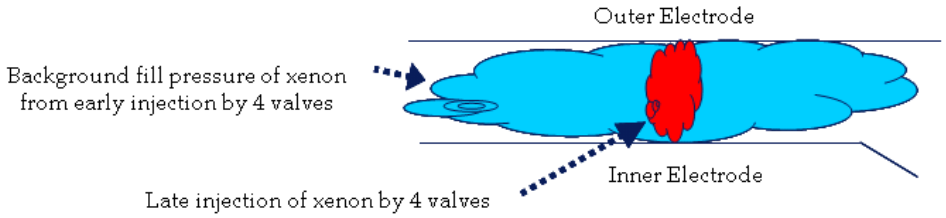

Figure 5.1: Illustration of background fill gas injection. Four of the outer gas puff valves inject gas early in time, 5 ms prior to voltage application, allowing more time for the neutral xenon to expand creating a background fill pressure. The other four outer gas puff valves inject gas late in time just before voltage is applied, creating a much smaller volume of dense gas to be ionized and accelerated.

In an attempt to increase the EUV and magnetic field production further, the line pressure was again reduced to 2000 torr, starting with the similar settings as shown in Table 3.1. The net result was lower EUV production and lower magnetic fields, indicating 3000 torr line pressure was a closer optimum, which had been found in the initial xenon survey without the EUV diagnostic as well.

The final part of the EUV emission survey focused on inner and outer gas puff time variation, at 6 kV, 3000 torr line pressure, and full gates. First GPB1 was held constant at -1.7 ms, GPB3 and GPB5 were held at -0.7 ms, while GPB2 and 4 were varied. After an extensive number of shots, it was determined earlier times yielded stronger magnetic fields and higher EUV emissions, as well as more quiescent pinches. An optimum was chosen at -5.3 ms for GPB2 and 4, but overall the timing change for GPB2 and 4 caused little change in production between -4 and -6 ms. With the optimum chosen for the outer gas puff timings, GPB1 was altered until the optimum output was reached at -2.6 ms for GPB1. A graph of the final inner gas puff timing survey versus average EUV diagnostic current output is given in Figure 5.2. The EUV diagnostic current was averaged from 24 to 40 μs, the period of the majority of the EUV production. The solid red trace shows the average value for a given gas puff timing, with the dashed black lines showing the standard deviation from the average caused by the discrete averages for each shot, shown as black

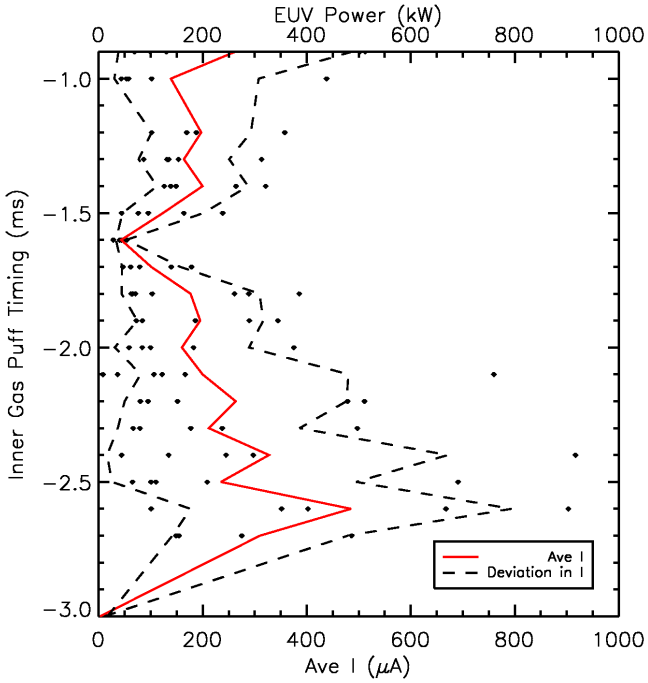

Figure 5.2: Average EUV emission results of the final timing survey, averaged from 24 to 40 μs. The solid red trace shows the average EUV current for a given time, and the black dashed lines show the standard deviation from the average. The black dots indicate individual average EUV current for a given shot. Since the PCF is roughly 1×10^9 W/A, and the current is given in μA, this graph also shows the average EUV power output in kW.

dots. Since the PCF from Equation 4.11 is roughly 1×10^9 W/A, and the average current is in μA, the total EUV power can be taken to be roughly the same number in kilowatts as the average EUV current in Figure 5.2, with a maximum average of approximately 500 kW of EUV power from the viewed Z-pinch from $z = 8.7$ cm to $z = 25.7$ cm. A total of 100 data shots were used in the inner gas puff timing survey pictured.

With the timing optimized to the fullest extent possible, the voltage and gate settings were altered, but plasma voltage spikes limited changes to either, and the optimum settings were taken to be at 6 kV charge voltage, and full gates. The optimum settings are listed in Table 5.1. A total of 653 data shots were taken during the EUV emission survey.

Table 5.1: Final ZaP optimum operating parameters for EUV emission from xenon plasmas.

parameter	value
capacitor bank configuration	Low inductance
charge voltage	6 kV
line pressure	3000 torr
Gas Puff Valve Gate	Full
T_{gpb1}	-2.6 ms
T_{gpb2}	-5.3 ms
T_{gpb3}	-0.7 ms
T_{gpb4}	-5.3 ms
T_{gpb5}	-0.7 ms
Average EUV emission between 24–100 μs	170 $\pm$ 110 kW
Average EUV emission between 24–40 μs	550 $\pm$ 390 kW

5.2 Accuracy of the EUV Diagnostic

Figure 5.3 shows graphs of the current waveform, magnetic field and mode data, as well as the EUV diagnostic and bolometer current output versus time. The EUV emission is highest when the magnetic field is at its max, indicating a small diameter, hot, Z-pinch. The EUV diagnostic output also follows the output of the bolometer, but has a different viewing geometry and QE, giving it roughly twice the output of the bolometer in the same wavelength range.

As mentioned in Chapter 4, the EUV diagnostic lacks a floating electrostatic shield, which can explain why the output current is positive from 20 to 24 μs. This positive output would appear to be due to the arrival of the plasma at the EUV diagnostic. The EUV diagnostic is located near the outer electrode where a hole cut in the outer electrode allows viewing of the plasma. When the current sheet accelerating the plasma first arrives at $z = 17$ cm, there is an opportunity for some of the plasma and current to attach outside the electrode, especially to the outside of the EUV shield which is in close proximity. Figure 5.4 shows a time contour of the magnetic field magnitude at a given z position. At $z = 17$ cm a vertical line is drawn to represent the position of the EUV diagnostic. From the figure, the magnetic field initially starts out at close to zero at 20 μs, but slowly rises as the pinch begins to form. When the pinch is completely formed, the magnetic field keeps the current sheet away from the diagnostic, and the signal is likely due only to EUV emissions. Considering this and how the EUV diagnostic current peaks appear to follow the bolometer current peaks, and knowing the bolometer has a floating electrostatic shield, it can be concluded the lack of a floating electrostatic shield has little impact on the accuracy of the EUV diagnostic after 24 μs.

5.3 Magnetic Field Effect on EUV Emission

The azimuthal magnetic probe arrays nearest the EUV diagnostic are at $z = 0$ and $z = 35$ cm, putting the EUV diagnostic directly between both arrays, and unable to view the pinch at either location. The EUV emissions, however, seem to follow the magnetic activity at

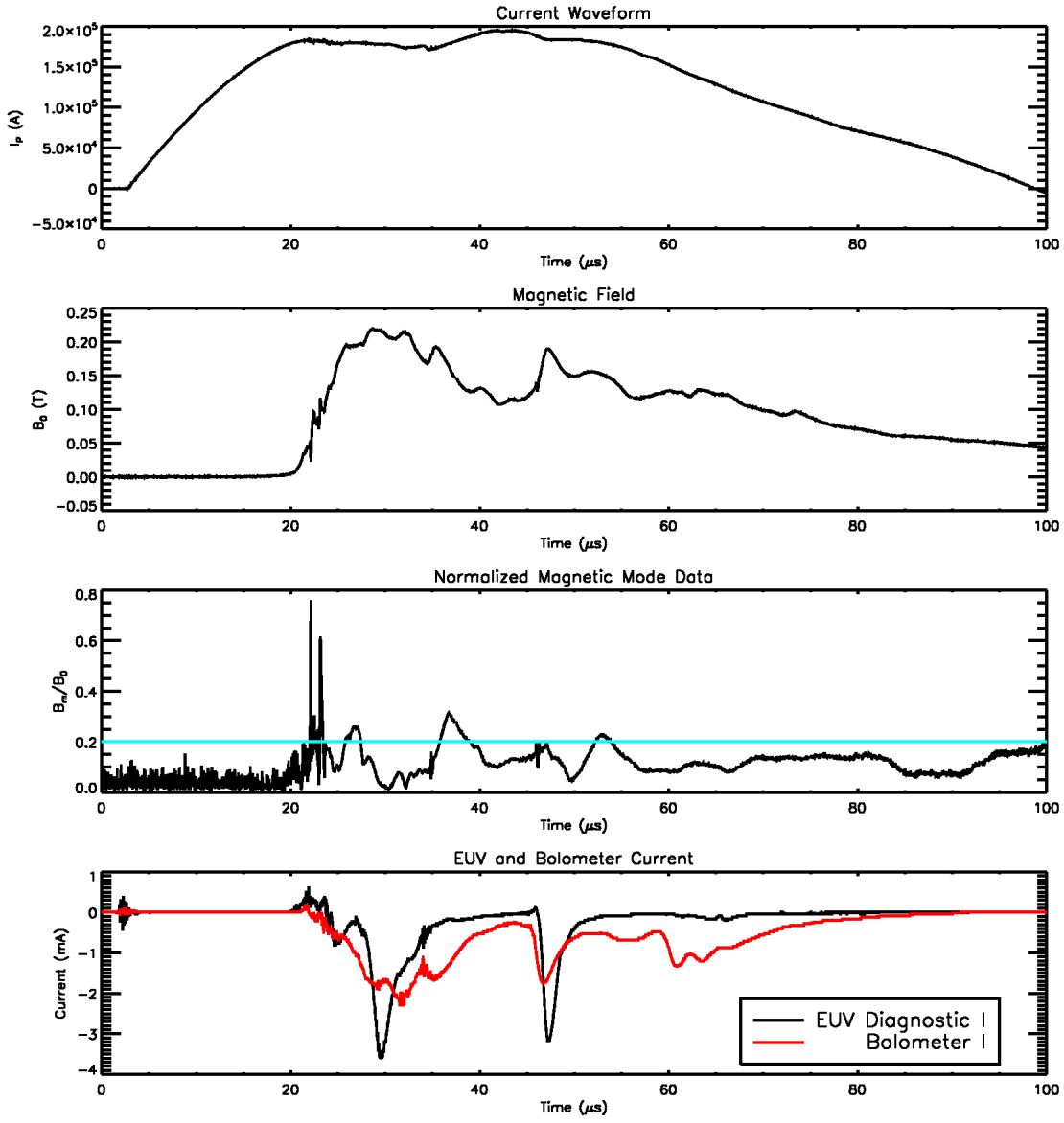

Figure 5.3: EUV emission comparison to magnetic field and mode data. The peak of the magnetic field at $z = 0$ shown in the second graph reaches 0.2 tesla (T) and is maintained there from 25 to 36 μs, with an additional peak starting after 46 μs, during which there are maximums in the EUV current output, as shown in the bottom graph. The bolometer current peaks matches the EUV diagnostic peaks, though the peaks are lower due to different viewing geometry and QE, indicating an accurate signal from the EUV diagnostic. The mode data at $z = 0$ also becomes its most quiescent during the same periods, indicating a quiescent, hot Z-pinch yields the greatest EUV output.

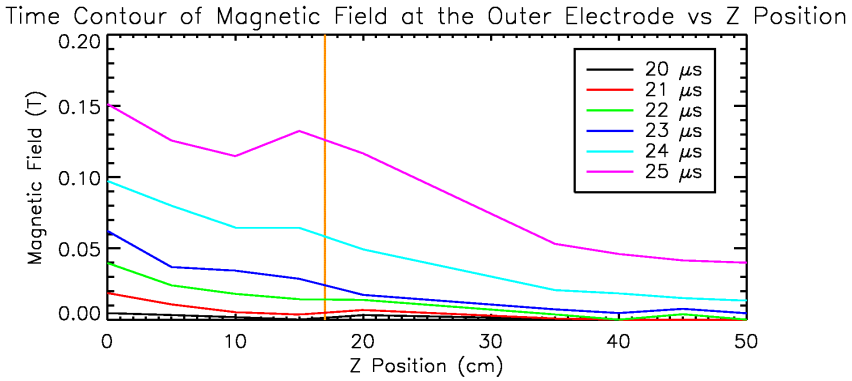

Figure 5.4: Arrival of plasma at the EUV diagnostic, shown as a time contour of the magnetic field magnitude at a given z position. At $z = 17$ cm a vertical line is drawn to represent the position of the EUV diagnostic. The magnetic field initially starts out at close to zero at 20 μs and slowly rises, indicating the plasma arrives at the EUV diagnostic between 20 and 24 μs, as the Z-pinch is forming, potentially attaching to the EUV diagnostic and giving a erroneous positive current signal during the same time frame, after which the Z-pinch keeps plasma away from the EUV diagnostic.

$z = 0$, and comparisons of EUV emissions to magnetic field will be referenced to $z = 0$. As seen in Figure 5.3, the xenon Z-pinch forms initially at 24 μs, has a temporary instability until 27 μs, then forms a very quiescent period up until a short lived, low magnitude instability occurs at 36 μs lasting until 39 μs before reforming a tight Z-pinch until a very low amplitude instability occurs at 55 μs, after which the magnetic field slowly falls off, though the pinch remains quiescent.

The EUV emission is highest roughly when the Z-pinch is most quiescent, and when the magnetic fields are highest. With this configuration, magnetic fields in the xenon Z-pinches reach the same maximum fields as seen in the hydrogen pinches in similar conditions, such as the one in Figure 3.12, and for similar durations. The peak of the magnetic field at $z = 0$ reaches 0.2 tesla (T) and is maintained there from 25 to 36 μs. The magnetic probes are located in the wall of the outer electrode. With the magnetic field dropping as the inverse of the radius, and the radius of the pinch being approximately 1 cm, the magnetic field just

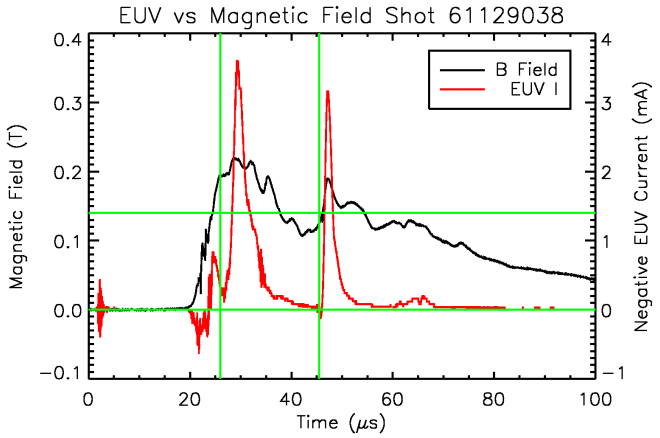

Figure 5.5: EUV emissions versus magnetic field. The two peaks in the magnetic field occur at the same time as the two peaks in EUV emissions, both of which occur when the magnetic mode data suggest the most quiescent, hottest pinch at 30 and 48 μs. The second peak in EUV emissions also begins at 46 μs just as the magnetic field reaches 0.14 T after reaching a minimum following the temporary instability between 36 and 39 μs.

outside the pinch must therefore be approximately 2 T at $z = 0$. A direct relation between EUV emission and magnitude of magnetic field is shown in Figure 5.5. The two peaks in the magnetic field as seen in Figure 5.3 occur at the same time as the two peaks in EUV emission, both of which occur when the magnetic mode data suggest the most quiescent, hottest pinch at 30 and 48 μs. The second peak in EUV emissions also begins at 46 μs just as the magnetic field reaches 0.14 T after reaching a minimum following the temporary instability between 36 and 39 μs. EUV emissions have been seen when the magnetic field never reaches 0.14 T, but higher magnetic fields tend to drive EUV emissions higher.

5.4 Spectrometer Data Comparison to EUV Emission

As noted in Chapter 3, the ICCD can also be used to make rough estimates of the size and temperature of the pinch [9, 10]. For xenon to emit EUV light at the desired 13.5 nm wavelength, xenon must be ionized 10 times to reach xenon XI. Unfortunately, xenon IX through XI do not have line radiation above the 200 nm wavelength which is lower

wavelength limit for both the CCD and ICCD spectrometers, and is therefore not visible to the PMT, either. Xenon VIII, however, does have line radiation at 212.22 nm, which is also in the vicinity of several line emissions from other, lower xenon ionizations states. Prior to the installation of the EUV diagnostic, line radiation at 218.7 nm was monitored by both the ICCD and CCD showing the presence of xenon IV ions. With the optimum parameters for generating EUV light established, a xenon VIII line has been detected at 212.22 nm, without the presence of lines from lower ionization states, indicating the pinch has reached high enough temperatures to burn through the lower ionization states. A xenon VIII line as measured by the ICCD is shown in Figure 5.6, again taken at 90 degrees to the z axis, at $z = 0$. The ICCD was set to trigger at 30 μs for a 100 ns gate, which happened during the most quiescent period, strongest magnetic field output of the pinch, and during the strongest EUV emissions. The less intense line at 213.5 nm is most likely a xenon VI line at 213.49 nm. Lower ionization states have lines in the region but are not visible. From this ICCD data, the pinch would be approximately 1.75 cm in radius, with the hottest portion being closer to 0.7 cm in radius.

In addition to the ICCD spectra, the PMT was set to monitor the time evolution of xenon VIII line at 212.2 nm during the same shot as in Figures 5.3 and 5.6, at $z = 10$ cm, a z location also viewed by the EUV diagnostic. The evolution of the xenon VIII signal versus the EUV emission is shown in Figure 5.7, where the PMT signal has arbitrary units with the relative magnitude of the signal being important. At 24 μs, the PMT signal increases indicating the presence of xenon VIII emissions at 212.2, but remains steady even after the EUV emission increases, indicating the xenon Z-pinch has burned through to higher ionization states of xenon [11]. The PMT signal again temporarily increases after the EUV signal decreases at 62 μs, and reaches a maximum at 70 μs before decreasing again, indicating the pinch is cooling, which is also supported by the steady decrease in current and magnetic field in the same time frame as seen in Figure 5.3, and in the small, steady increase in the magnetic mode data.

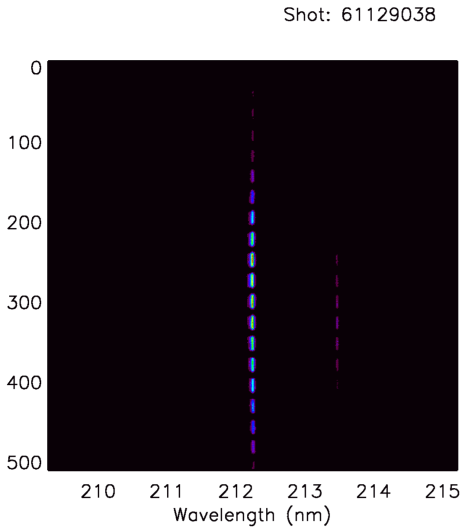

Figure 5.6: ICCD spectra of a xenon VIII ion at 212.22 nm. The ICCD was set to trigger at 30 μs, which happened during the most quiescent period, strongest magnetic field output of the pinch, and during the strongest EUV emissions. The less intense line at 213.5 nm is most likely a xenon VI line at 213.49 nm. Lower ionization states have lines in the region but are not visible, indicating the Z-pinch has burned through these states.

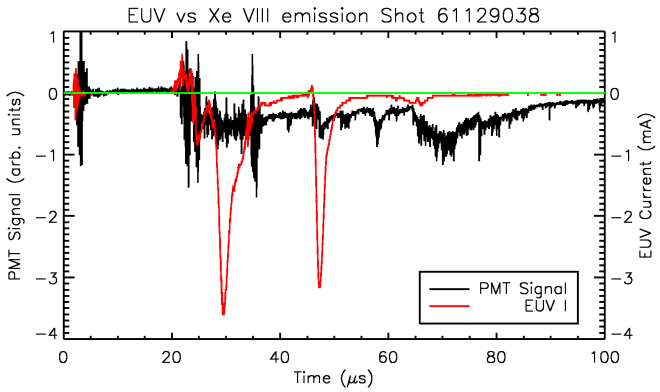

Figure 5.7: EUV emission versus xenon VIII emission at 212.2 nm as measured by the PMT at $z = 10$. At 24 μs, the PMT signal increases indicating the presence of xenon VIII emissions at 212.2, but remains steady even after the EUV emission increases, indicating the xenon Z-pinch has burned through to higher ionization states of xenon. The PMT signal again temporarily increases after the EUV signal decreases at 62 μs, and reaches a maximum at 70 μs before decreasing again, indicating the pinch is cooling.

5.5 Summary of the EUV Emission Survey

The EUV diagnostic has functioned effectively during the EUV emission survey, even without the benefit of a floating electrostatic shield. Optimum operating parameters for EUV emission from xenon Z-pinches have been determined as shown in Table 5.1. A maximum average EUV power output of 550 kW, from the EUV diagnostic-viewed Z-pinch from $z = 8.7$ cm to $z = 25.7$ cm, in the 11 to 18 nm wavelength range, has been found when the current output of the EUV diagnostic is averaged over the period between 24 and 40 μs. ICCD and PMT data supports the burn through to ionization states above xenon VIII, which would indicate a contribution to EUV emission from xenon IX to xenon XI is very likely. A final comparison of the ZaP EUV emissions versus other popular sources for EUV lithography is given in the final chapter.

Chapter 6

EVALUATION OF THE ZAP FLOW Z-PINCH AS AN EUV LITHOGRAPHY LIGHT SOURCE

6.1 Comparison of the Flow Z-Pinch to current EUV light sources

As mentioned in the introduction, the current EUV light power requirement into 2π sr is 400 W for LPPs and 1200 W for GDPPs [5]. This corresponds to a 180 W power at the intermediate focus of the source collector, or to a requirement of 10 mJ/cm^2 of deposited energy into the photoresist expected to be used in EUV lithography [3].

The PCF is based on power into 4π sr, therefore to make an equal comparison, the power outputs shown previously need to be divided by 2. From Table 5.1, the maximum average EUV light power output of the Flow Z-Pinch into 2π sr is 280 kW for 16 μs or 90 kW for 76 μs for the viewed volume of plasma, or 17.4 cm section of the pinch. If all the EUV light can be focused to 1 cm^2, the total deposited EUV energy from one pulse is 4.50 J in 16 μs or 6.80 J in 76 μs, 450 and 680 times more energy than is needed, respectively. If the lower limit is used from Table 5.1, the average EUV power output from the 17.4 cm viewed pinch into 2π sr is 80 kW for 16 μs or 30 kW for 76 μs, yielding a deposited energy of 3.70 J and and 2.30 J, still hundreds of times greater than the amount of energy needed. At ZaP's highest EUV power output of nearly 940 kW for 16 μs, 15 J of energy can be deposited per cm^2.

By comparison, if all the EUV power can be focused from a 100 ns duration pulse of a LPP or GDPP, the total energy deposited is 40 μJ for an LPP, requiring 250 pulses to reach the required energy, or 0.12 mJ for an GDPP, requiring 83 pulses to reach the required energy deposition [3, 7]. Both values are 19,000 times or more smaller than the energy deposition already attained in the Flow Z-Pinch. Even if the collection efficiency is as low as it is in the GDPP case, the Flow Z-Pinch can theoretically deposit 340 mJ/cm^2 at its

lowest output, 34 times more energy than is required, and in only one pulse.

Additionally, the measured EUV power comes from only 17.4 cm of the pinch. Over 25 cm of the pinch upstream from the pinch viewed by the EUV diagnostic has not been measured, and that portion of the pinch is the hottest part of the plasma. The total EUV emission from the entire Z-pinch is likely double if not greater than what is measured by the EUV diagnostic.

This assumes that all the EUV light measured is at the 13.5 nm wavelength. With a pass band between 11–18 nm on the EUV diagnostic, the actual wavelength cannot be known with certainty. Additional diagnostics or narrower pass band photodiodes are needed to be certain of the actual wavelength emitted.

Based on the present information, however, the ZaP Flow Z-Pinch experiment is a promising EUV light source for lithography, if properly scaled for efficient power use and wavelength production, and with the proper collection optics. The duration of the EUV light emission is 140 times longer than any other current EUV light source, with a total EUV energy output 19,000 times greater than other EUV light sources. The EUV energy deposited by just one pulse of the Flow Z-Pinch is more than sufficient for the projected EUV photoresist requirements in EUV lithography.

6.2 Future Work

Enough material is available currently to construct a second EUV diagnostic. Another diagnostic will allow the study of EUV light emission at multiple locations throughout the pinch simultaneously. Future EUV diagnostics should also include a floating electrostatic shield for maximum accuracy. A narrower pass band photodiode can also be installed on the current and future EUV diagnostics to reduce the possible EUV light emissions to a smaller band of light. A photodiode amplifier has been purchased which will be able to properly amplify the weaker signal from the lower QE, narrow pass band photodiodes. Other diagnostics sensitive to the EUV wavelength range can also be used to evaluate the total power output near 13.5 nm.

Continued optimization of the Flow Z-Pinch operating parameters may also yield higher, more consistent EUV power output. The use of a voltage snubber device can minimize the plasma voltage instabilities, and allow higher charge voltages to be applied. Currently, a new inner electrode has been designed and built, and is awaiting installation into ZaP. This new inner electrode has a larger diameter, 30 cm as compared to 20 cm of the current inner electrode, and will require the plasma to collapse from a greater distance from axis, resulting in greater heating of the Z-pinch, which can also lead to greater EUV output.

Finally, an evaluation of ZaP's EUV output should be conducted with one of the semiconductor industry-standard diagnostics. This would give a direct relation between ZaP's measured EUV power output, and its viability as an EUV lithography light source.

BIBLIOGRAPHY

[1] M. Kanellos. IBM promotes making chips in the Bath. CNET News.com, 2/21/06.

[2] P.J. Silverman. Extreme ultraviolet lithography: overview and development status. *Journal of Microlithography, Microfabrication, and Microsystems*, 4(1):11006 – 1, January 2005.

[3] Bjorn A. M. Hansson, Igor V. Fomenkov, Norbert R. Bowering, Alex I. Ershov, William N. Partlo, David W. Myers, Oleh V. Khodykin, Alexander N. Bykanov, Curtis L. Rettig, Jerzy R. Hoffman, Ernesto Vargas L., Rod D. Simmons, Juan A. Chavez, William F. Marx, and David C. Brandt. LPP EUV source development for HVM. In Michael J. Lercel, editor, *Emerging Lithographic Technologies X*, volume 6151, page 61510R. Proceedings of the SPIE - The International Society for Optical Engineering, 2006.

[4] U. Stamm, J. Kleinschmidt, D. Bolshukhin, J. Brudermann, G. Hergenhan, V. Korobotchko, B. Nikolaus, M. C. Schurmann, G. Schriever, C. Ziener, and V. M. Borisov. Development status of EUV sources for use in beta-tools and high-volume chip manufacturing tools. In Michael J. Lercel, editor, *Emerging Lithographic Technologies X*, volume 6151, page 61510O. Proceedings of the SPIE - The International Society for Optical Engineering, 2006.

[5] U. Stamm, J. Kleinschmidt, K. Gabel, G. Hergenhan, C. Ziener, G. Schriever, I. Ahmad, D. Bolshukhin, J. Brudermann, R. de Bruljn, T.D. Chin, A. Geier, S. Gotze, A. Keller, V. Korobotchko, B. Mader, J. Ringling, and T. Brauner. EUV sources for EUV lithography in alpha-, beta- and high volume chip manufacturing: An update on GDPP and LPP technology. *Proceedings of the SPIE - The International Society for Optical Engineering*, 5751(1):255 – 66, 2005.

[6] U. Stamm. Extreme ultraviolet light sources for use in semiconductor lithography-state of the art and future development. *Journal of Physics D (Applied Physics)*, 37(23):3244 – 53, December, 07 2004.

[7] U. Stamm, I. Ahmad, I. Balogh, H. Birner, D. Bolshukhin, J. Brudermann, S. Enke, F. Flohrer, K. Gabel, S. Gotze, G. Hergenhan, J. Kleinschmidt, D. Klopfel, V. Korobotchko, J. Ringling, G. Schriever, C.D. Tran, and C. Ziener. High-power euv lithography sources based on gas discharges and laser-produced plasmas. *Proceedings of the SPIE - The International Society for Optical Engineering*, 5037:119 – 29, 2003.

[8] U. Shumlak, B. A. Nelson, C. S. Adams, D. J. Den Hartog, R. P. Golingo, S. L. Jackson, S. D. Knecht, J. B. Pasko, and D. T. Schmuland. Equilibrium Evolution in the ZaP Flow Z-Pinch. *Journal of Fusion Energy*, 10.1007/s10894-006-9031-8:1–5, December 7 2006.

[9] R. P. Golingo, U. Shumlak, and B. A. Nelson. Formation of a sheared flow Z pinch. *Physics of Plasmas*, 12(6):62505 – 1, June 2005.

[10] U. Shumlak, R. P. Golingo, B. A. Nelson, and D. J. Den Hartog. Evidence of Stabilization in the Z-Pinch. *Physical Review Letters*, 87(20):205005/1–4, November 2001.

[11] U. Shumlak, B. A. Nelson, R. P. Golingo, S. L. Jackson, E. A. Crawford, and D. J. Den Hartog. Sheared flow stabilization experiments in the ZaP flow Z pinch. *Physics of Plasmas*, 10(5):1683 – 90, May 2003.